Development of novel mosaic adeno-associated virus vector for stable manipulation and imaging of neural activity in nonhuman primate brains

霊長類脳における
神経活動の操作やイメージングに適した
新規モザイクアデノ随伴ウイルスベクター
の開発

Kyoto University Graduate School of Science
京都大学大学院理学研究科

Kei Kimura

木村　慧

2023

Table of contents

General Introduction

1.1. Neural circuit manipulation techniques in primate brain

The brain consists of the complex neural networks constituting numbers of neurons that communicate with one another. Neuroscientists have made various efforts over a hundred many years to elucidate the brain networks, including investigations of neural network connectivity through neuroanatomical tracing and neurophysiological recording. Aiming to obtain a comprehensive understanding of brain functions, large-scale research projects have been initiated worldwide[1]. Through the accumulation of research findings, our understanding of the brain structure and function is advancing rapidly. These include studies examining the detailed structure of whole brain and investigations into the relationships between individual brain regions and their functions. However, there is still room for research in understanding the relationship between the anatomical connectivity and brain function, particularly focusing on the functions of individual neural circuits. To elucidate the higher brain functions that integrate complex mental processes, it is crucial to focus not only on the functions of individual brain regions but also on the neural circuits connected with multiple regions. To explore the function of a specific neural circuit, it is necessary to precisely control the activity of that circuit and investigate the effects on both the neural activity in circuits receiving projections from it and on behavior.

There are three broad categories of methods for manipulating neuronal circuit activity: electrical stimulations, neuropharmacological manipulations, and genetic engineering methods. Electrical stimulations of neurons have the advantage of manipulating neuronal activity with high temporal resolution. However, it is hard to manipulate neuronal activity limited to neurons receiving projections from a specific brain region because the surrounding neuronal population is also affected by electrical stimulation.

Neuropharmacological manipulations alter neuronal activity by using agonists and antagonists that act on specific receptors of neurons, inducing excitatory or inhibitory responses in the affected neurons, respectively. The advantage of this method is that the effects of changes in neural activity on behavior can be examined from the perspective of changes in the dynamics of specific neurotransmitters. Compared to the electrical stimulation, the effect of stimulation lasts for a longer period of time and the temporal resolution of the timing of stimulation is lower. Also, as with electrical stimulation, it is difficult to limit the extent of drug effects based on connectivity with specific brain regions. One promising candidate to solve the problems common to both electrical and pharmacological stimulation methods is the manipulation of neural circuits by optogenetic pathway-selective stimulation. Optogenetics is a technique in which opsins are expressed on the plasma membrane of neurons, thereby sensitizing neurons to specific wavelengths of light and controlling neuronal excitability[2-4]. It is possible to control the activity of a specific projection system through axonal stimulation by applying light stimulation to one of the projection sites of opsin-expressing neurons. Manipulation of neural activity by optogenetics, like the electrical stimulation method, is performed with high temporal resolution, making it possible to intervene in the activity of a specific neural circuit at the timing of an action[2-4]. Selective manipulation of neural pathway activity by optogenetics may be a more direct method for causally analyzing the function and information processing of targeted neural circuits.

As represented by optogenetics, innovative techniques for gene transfer into neurons have brought a variety of new research methods to the field of neuroscience research[5-9]. Chemogenetics is another method that has emerged in recent years as a powerful tool for circuit manipulation approaches in the field of neuroscience research. In chemogenetics,

artificial receptor proteins designed to interact with specific agonists are introduced into target neurons[5-9]. Only when the agonist is administered and binds to the artificial receptor does the excitability of the neural activity change. Chemogenetic stimulation methods, like pharmacological stimulation methods, produce lasting effects over a period of time, but can also be manipulated in the pathway-selective manner, as in optogenetics[10,11]. The combination of genetic engineering and neuroscience has also enabled the monitoring of neural activity at high spatial resolution from a wide range of areas. Calcium imaging methods use fluorescence imaging to measure changes in calcium ion concentrations resulting from neural activity. Neurons expressing calcium ion indicator proteins undergo changes in intracellular calcium ion concentration, resulting in a transient change in fluorescence during neuronal activity. By capturing this change in fluorescence through multiphoton excitation microscopy, it is possible to measure the cellular or subcellular level (cell body, dendrites, and axons) from a wide area with high spatial resolution[12].

Although the development of such genetic manipulation techniques has been actively pursued using rodents, it is essential to use non-human primates (NHPs) to manipulate neural networks in order to elucidate the relationship between human neural networks and brain function. Nonhuman primates are useful as model animals for neuroscience research because of their evolutionary closeness to humans, their ability to perform complex tasks, and their brain structure similarity to humans. Nevertheless, research on the manipulation of neural circuits using genetic techniques in primates is very limited compared to that in rodents. In order to introduce genes for functional molecules into neurons of the primate brain, applicable viral vectors must be developed. First, because primate brains have more complex immune systems than rodents, introduced foreign proteins can cause serious immune reactions in the primate brain, even if they are not

harmful to the rodent brain[13,14]. Second, there are cases in which transgene expression property of viral vector differs between rodents and primates[13]. Third, because the use of genetically modified animal models such as transgenic or knock-in models, is still difficult in primates, the infectivity to specific cell types have to be achieved by the inherent characteristics of the viral vector itself. Therefore, the improvement and optimization of viral vector are most important for pathway-selective gene manipulation and neural activity imaging in primates.

1.2. Viral vectors for neural circuit manipulation in primates

Variety of viral vectors are currently available for manipulating and imaging of neural activity in the primate brain. Lentiviruses and adeno-associated virus (AAV) vectors are well known and often used in research on neural circuit manipulation in primates and rodents. Lentiviral vectors originating from human immunodeficiency virus type 1 (HIV-1) are a strong candidate for gene transfer. There are three main reasons: 1) permanent and stable transgene expression achieved by insertion of transgene into the host chromosome; 2) efficient infection in both dividing and non-dividing cells; and 3) a large capacity for the genome size of transgene (Figure 1-1). While lentiviral vector is capable of long-term gene expression, there is a potential for oncogenesis derived from their insertion into the host genome[15]. Although lentiviral vector is considered to have low cytotoxicity due to their replication-deficient forms[16,17], the less neuron-specific types of lentiviral vector can cause immune reactions at the site of infection[14]. Moreover, lentiviruses are enveloped viruses with their viral components surrounded by a lipidic bilayer (envelope). Enveloped viruses, which are easily destroyed by ethanol or surfactants, are less stable than viruses without envelopes[18]. AAV, another strong candidate for gene transfer to primates, is a stable non-enveloped virus (Fig. 1-1). The outer shell of AAV is composed of capsid proteins which are formed as an icosahedral structure. As well as lentiviral vectors, AAV vectors have lost most of their original viral genome and have low immunogenicity[19]. The disadvantage of AAV is small genetic capacity that can be carried[20,21]. However, unlike many other viral vectors including lentiviral vectors, AAV vectors can be handled at biosafety level 1 (BSL1). For these reasons, AAV vectors are widely used by many researchers for neural circuit manipulation experiments in primates[10,22-35].

1.3. Inflammatory responses induced by virus vectors in primate brain

Over the past ten years, researchers have attempted to apply the technique of optogenetics, chemogenetics, and calcium imaging to nonhuman primates[7,8,36]. While these techniques have been developed using rodents, they have recently become applicable to primates as well. However, the straightforward application of viral vectors developed in rodents to primates does not always yield successful results, as the influence of viral vectors can differ between primates and rodents. For instance, in the previous research, the same viral vector expressing a fluorescent protein was injected into the brains of macaques and rats, and their inflammatory responses were compared[14]. When comparing brain slices subjected to Nissl staining at the injection site, it was found that there was no inflammation in rats, while macaques exhibited tissue degeneration. Inflammatory markers, such as Iba1 and CD8, showed no response in rats but a significant response in macaques. This example illustrates species-specific differences in the influence of viral vectors, emphasizing the need to reevaluate their behavior in the brains of primates, even if they have proven highly useful in rodents.

Even in AAV, which is known for its relatively low inflammatory properties, there have been reports of inflammation following intracerebral injection. It is known that the AAV has various strains called as "serotypes," each exhibiting distinct infection tropisms and transgene expression properties based on their own serotype. For example, AAV9 infects not only neurons but also glial cells upon intracerebral injection, indicating low neuronal specificity, as reported in previous studies[37]. In contrast, AAV2 is highly neuron-specific, primarily infecting neurons, and is believed to induce little to no inflammation. It is known that the microglia play a role in the immune function in the brain. The AAV9 vector, which infects glial cells, has been suggested to recruit

antigen-presenting cells and induce immune responses within the brain in both primates and rodents[38,39]. Based on these prior studies, vectors with low neuronal specificity are considered to carry potential risks for triggering inflammation in the brain. Therefore, in order to avoid inflammatory reactions, it is necessary to use vectors with high neuronal specificity.

1.4. Optimal properties for stable manipulation and imaging of neural activity in nonhuman primate brains

What type of AAV vector should be used in primates? In the previous studies, several serotypes of AAV vectors have been used in primate brains, however, the choices of serotypes are still divided among researchers. To determine which serotypes, promoters, and opsins are efficient in macaque monkey brains, Tamura et al. examined 13 AAV serotypes or properties at the preliminary steps of their experiments for optogenetic neural manipulation in the perirhinal cortex of macaque monkeys[35]. Even though they have indicated one of the best AAV vector's properties for their conditions of optogenetic manipulation at the perirhinal cortex of primates, researchers are still struggling to seek their own optimal properties of AAV vectors. If they examined the different target of brain regions, transgenes, promoters, and so on, the better property of AAV vector could be changed. Unfortunately, comprehensive studies about choice of AAV vectors for neural circuit manipulation in primate brains are very rare. To break through this inefficient situation in primate neuroscience research, the AAV vector that can be commonly used for various purposes and that are practical not only for rodents but also for primate brains is highly desired.

What is the optimal property of AAV vectors for primate brains? As per the previous section, inflammatory responses are more likely to be induced by AAV vectors in primate brains. The lower toxicity is one of the important properties for the optimal property of AAV vectors for primates, and the neuron specific infectivity is also crucial for avoiding immune response in the brain. The efficiency of gene transduction of AAV vectors is also important for neural circuit manipulations. Although the recombinant AAV2 vectors are widely used for the neuroscience research field, the transgene

expression levels of AAV2 vectors are often not enough for inducing behavioral changes by neural circuit manipulations. My colleagues have reported that both optogenetic and chemogenetic neural manipulations on macaque monkeys by using the AAV2 vectors successfully modulated behaviors[29,33]. However, these cases are exceptions, and most researchers tend to use other serotypes of AAV vectors which has higher transgene expression properties, such as the AAV1, 5, 8, 9 vectors[22-28,30-31,34,35]. Watakabe et al. compared transgene expression levels and toxicity for neurons among 5 serotypes of AAV vectors in both rodents and primates[13]. They clearly showed that the transgene expression levels were different among the serotypes, and the AAV1, 5, 8, 9 vectors showed higher levels of transgene expression but the AAV2 vector presented significantly lower transgene expression levels in macaque monkeys and marmosets. However, the AAV vectors which has higher transgene expression properties has the possibility to induce general toxic effects on neurons. Watakabe et al. also reported that the transduced regions of the AAV8 vectors in marmoset brain exhibited heavy accumulation of glial cells. Such glial accumulations were not observed for AAV1, however, they also observed same infiltration of glial cells into the injection site of the AAV1 and AAV9 vectors when they extended the survival time from 3 weeks to 6 weeks after the injection date. Especially for the AAV9 vectors, such immune responses were reported in some previous studies[37-39]. Since glial cells are involved in immune responses[40], using viral vectors with neuron-specificity could potentially be effective in preventing the induction of immune responses. However, the AAV vector that combine high gene transduction efficiency with low immunoreactivity did not exist, and the development of a novel AAV vector which has both characteristics is desired.

11

1.5. Seeking for novel AAV valiant with desired characteristics

There are several approaches to altering the properties of AAV vectors. Directed evolution is one of the approaches to change the viral capsid by genome mutation and selection pressure[41]. Random mutations are inserted into the viral capsid sequence, and AAVs with the desired properties are found by screening process. The capsid sequence of the recombinant AAV vector is integrated into the viral genome, thereby allowing the viral genome to be packaged by its own capsid. Therefore, the genome of a screened virus can be examined to determine which capsid variants have superior characteristics among the randomly generated variants. Further random mutations are caused around capsid sequence of AAV variant showing superior characteristics obtained in screening process, and the screening can be repeated to obtain better characterized variants. To create the AAV vector with specificity for microglia, multiple random amino acids were inserted between amino acids in the capsid protein of AAV9[42]. Through the multiple screening process by using the cultured microglia, the candidate of AAV variant with the ability to infect microglia was selected. This method is particularly useful for creating the AAV vectors with characteristics not found in conventional AAV vectors, such as retrograde infection and effectively crossing blood-brain barrier. AAV2-retro, the AAV variant which has retrograde infectivity, was also created by using directed evolution[41,43]. AAV-PHP.eB, a powerful AAV variant for widespread gene transfer into the whole brain region via intravenous injection, was also developed through the method developed from directed evolution[44,45].

On the other hand, there is an approach to create the AAV vectors with mosaic capsid that utilize the characteristics of conventional AAV vectors[46,47]. Mosaic AAV vectors are the AAV vectors composed of the mixture of capsid proteins derived from multiple

existing serotypes (Fig.1-2). The vectors may have the potential to combine the characteristics of each serotype due to the combination of different capsid proteins. For example, in a previous study, the mosaic vectors of AAV1 and AAV2 were created to develop the AAV vectors that exhibit high gene transduction efficiency to the liver and muscle[46]. As mentioned in earlier section, it is known that the AAVs have multiple serotypes with different infection tropism; AAV1 is known to have high gene transfer efficiency to muscle, and AAV2 is known to have higher gene transfer efficiency to the liver than AAV1. In the previous study, it was indicated that the mosaic AAV vector with 50% AAV1 capsid and 50% AAV2 capsid has a high gene transfer efficiency to both liver and muscle. Thus, by combining the capsid of the conventional serotype, a mosaic AAV vector may be obtained that has the superior characteristics to both conventional AAV vectors.

In seeking for the AAV vectors with new characteristics, the approach to be taken depends on whether the target property is novel or combines the characteristics of existing serotypes. For example, the "neuron-specific infectiousness" of AAV, as described in the inflammatory properties of AAV, is a feature of the existing serotype, AAV2, and can be combined with other features by creating mosaic vectors without searching by directed evolution. In addition, the "high efficiency of transgene expression" is also a property of several existing serotypes. Thus, it is concluded that the novel AAV vector which has both high efficiency of gene transduction and neuron specificity is able to be developed by developing the mosaic AAV vector.

1.6. Outline of the Thesis

According to these backgrounds, a mosaic AAV vector which has high levels of transgene expression capacity and neuron-specific infectivity was developed. A novel AAV vector, called AAV2.1 vector, in which capsid was composed of capsid proteins derived from both AAV1 and AAV2 was produced. In chapter 2, the properties between the AAV2.1 vector and several conventional AAV vectors were compared in the first series of experiments. Both the AAV2.1 vectors and the other AAV vectors were injected into the cerebral cortex of macaque monkeys and compared their transgene expression capacity and neuron specificity. The properties of the AAV2.1 vector were examined in the rat brains as well as in the macaque monkey brains. Through these investigations, it is indicated that the AAV2.1-A vector, composed of the mosaic capsid with a high ratio of AAV2 capsid protein (10% AAV1 and 90% AAV2), demonstrated the two optimal characteristics: high levels of transgene expression and neuron specificity. In the second series of experiments, the AAV vectors carrying the DREADD receptor were prepared and examined whether the AAV2.1 vectors is applicable for chemogenetic manipulation of neuronal activity in macaque monkeys. Furthermore, as the third series of experiments, *in vivo* calcium imaging was carried out in the visual cortex of macaque monkeys by using the AAV2.1 vector. These experiments confirmed the wide applicability of the AAV2.1 vector in the primate brain. The results from the present study will provide a novel candidate of viral vector with prominent characteristics for neuronal activity manipulation and imaging in primates.

Chapter 2: The mosaic AAV vectors enabled neuron-specific efficient gene transduction in the primate brain

2.1. Introduction

In recent years, much attention has been attracted to manipulating activity of neurons and their circuitry by gene transduction with viral vectors[48-50]. Recombinant adeno-associated virus (AAV) vector has particularly been utilized for a variety of cutting-edge techniques, such as optogenetics and chemogenetics (for reviews, see refs. 8, 51, 52). Indeed, substantial advances have been made in AAV vector-mediated gene transfer into target neuronal populations, and the validity of this strategy has been revealed in the primate brain as well as in the rodent brain[23-26,33,53,54]. It is generally accepted that the AAV has numbers of serotypes, and that individual serotypes show different infectious properties[55,56]. In gene transfer experiments on the primate and rodent brains, vectors based on the AAV serotypes 1, 5, and 9 (AAV1, AAV5, and AAV9) have so far frequently been used. These neurotropic AAV vectors exhibit higher levels of transgene expression than other serotype vectors, and, therefore, they may have been expected to exert adequate effects on modulating neuronal activity and animal's behavior[25,30,34,35,57]. However, given that such vectors possess considerable infectivity to glial cells as well as to neurons, there seems to be a serious pitfall that they cause inflammatory responses due to the glial infection[13,58-60].

In contrast, the AAV serotype 2 (AAV2) displays extremely high neuron specificity and, hence, low tissue damage[61-64]. Currently, recombinant vectors based on AAV2 are widely available for clinical use. Previous works have demonstrated in macaque monkeys that optogenetic/chemogenetic manipulations mediated through the AAV2 vector successfully modulated oculomotor/cognitive behaviors of the animals as well as related

neuron/pathway activities[29,33]. However, these reports are rather exceptional on account of a lower transgene expression capacity of the AAV2 vector compared with other serotype vectors[13,59]. Thus, various serotypes of AAV vectors are being utilized in world-wide laboratories for gene transfer experiments, especially on the primate brain, and many neuroscientists are still seeking for an AAV vector optimal for monitoring and manipulating target neuron/pathway activity. Conceivably, there is usually a trade-off relationship between the transgene expression capacity (i.e., sensitivity) and the neuron-specific infectivity (i.e., specificity). For improving the quality of gene transduction into the primate brain for diverse purposes, it is essential to create a novel AAV vector with marked superiority in both aspects.

Here, an AAV vector of which capsid was composed of capsid proteins derived from both AAV1 and AAV2 was developed. This mosaic vector, termed AAV2.1 vector, was designed to exhibit the excellence in transgene expression (for the AAV1 vector) and neuron specificity (for the AAV2 vector) simultaneously. By comparing with those of the original AAV2 and AAV1 vectors, the gene transduction property of the AAV2.1 vector following injections of these vectors into the frontal cortex of macaque monkeys was analyzed. Furthermore, the AAV2.1 vector property for gene transfer in comparison with the properties of AAV5 and AAV9 vectors was examined. In the present study, not only the transgene expression pattern of this mosaic vector, but also its applicability to chemogenetic manipulation and *in vivo* calcium imaging was explored in the striatum and visual cortex, respectively.

2.2. Methods

Animals

Eight adult macaque monkeys were used for three sets of our experiments (Monkeys A-H in Table 1): two rhesus monkeys (*Macaca mulatta*), 8 and 18 years old, females, 5.6 and 7.8 kg; one cynomolgus monkey (*Macaca fascicularis*), 4 years old, male, 5.2 kg; five Japanese monkeys (*Macaca fuscata*), 3-12 years old, one male and four females, 5.3-8.3 kg.

For the first set of our experiments with Monkeys A-D on gene transduction properties of mosaic AAV vectors, the experimental protocol was approved by the Animal Welfare and Animal Care Committee of the Primate Research Institute, Kyoto University (Permission Number: 2018-046), and all experiments were conducted according to the Guidelines for Care and Use of Nonhuman Primates established by the Primate Research Institute, Kyoto University (2010). For the second set of our experiments with Monkeys E and F on application of AAV2.1-A vector to chemogenetic manipulation, the experimental protocol was approved by the Animal Ethics Committee of the National Institutes for Quantum Science and Technology (Permission Number: 11-1038-11), and all experiments were conducted in accordance with the Guide for the Care and Use of Nonhuman Primates in Neuroscience Research (Japan Neuroscience Society; https://www.jnss.org/en/animal_primates). For the third set of our experiments with Monkeys G and H on application of AAV2.1-A vector to *in vivo* calcium imaging, the experimental protocol was approved by the Animal Experiment Committee of Osaka University (Permission Number: FBS-18-005), and all experiments were conducted according to the Guidelines for Animal Experiments established by Osaka University.

Viral vector production

All AAV vectors were produced by the helper-free triple transfection procedure. Briefly, AAV-293 cells (70% confluent in Corning Cell Stack 10 chamber) were transfected by genome, helper (pHelper; Agilent Technologies, California, USA), and packaging plasmids (pAAV-RC1, pAAV-RC2, pAAV-RC5, and pAAV-RC9) with polyethylenimine (PEI Max; Polysciences, Warrington, USA). For production of AAV2.1-A or AAV2.1-B vector, the pAAV-RC1 plasmid-coding AAV1 capsid protein and the pAAV-RC2 plasmid-coding AAV2 capsid protein were transfected respectively with the ratio of 1:9 or 5:5[46,47,65]. The AAV1, AAV2.1-A/B, and AAV2 vectors were then purified by affinity chromatography (GE Healthcare, Chicago, USA), concentrated to 150 µl by ultrafiltration (Amicon Ultra-4 10K MWCO; Millipore, Billerica, USA). AAV5 and AAV9 vectors were purified by CsCl gradient and concentrated to the same volume by ultrafiltration. The titer of each vector stock was determined by quantitative PCR using Taq-Man technology (Life Technologies, Waltham, USA). Viral solutions were diluted in 0.1 M phosphate-buffered saline (PBS; pH 7.4) containing 0.001% Pluronic F-80 (Sigma-Aldrich, St. Louis, USA) prior to injection.

The transfer plasmid (pAAV-CMV-mKO1-WPRE) was constructed by inserting the mKO1 gene (MBL Lifescience, Tokyo, Japan) and the WPRE sequence into an AAV backbone plasmid (pAAV-CMV; Agilent Technologies). The pAAV-hSyn-mKO1-WPRE plasmid was constructed by replacing the CMV promoter with the human Synapsin promoter, and, further, the pAAV-Syn-hM3Dq-WPRE plasmid was constructed by replacing the mKO1 gene with the hM3Dq gene. The method for construction of the pAAV-Syn-hM3Dq-IRES-AcGFP-WPRE plasmid was reported elsewhere[33,66], and the pAAV-CMV-hM4Di-IRES-AcGFP-WPRE plasmid was constructed by promoter

replacement as described above. The pAAV-CaMKIIα/hSyn-GCaMP6s-WPRE plasmid was constructed by replacing the CMV promoter and the mKO1 gene of the pAAV-CMV-mKO1-WPRE plasmid with the mouse CaMKIIα promoter (0.4 k base pair) or human synapsin promoter and the GCaMP6s gene.

Cortical injections of viral vectors

Four monkeys (Monkeys A-D in Table 1) were initially sedated with ketamine hydrochloride (5 mg/kg, i.m.) and xylazine hydrochloride (0.5 mg/kg, i.m.), and then anesthetized with sodium pentobarbital (20 mg/kg, i.v.) or propofol (5 mg/kg/hr). An antibiotic (Ceftazidime; 25 mg/kg, i.v.) was administered at the initial anesthesia. After removal of a skull portion over the frontal lobe, twelve different types of AAV vectors expressing RFP were injected bilaterally into the medial wall of the frontal lobe by the aid of a magnetic resonance imaging (MRI)-guided navigation system (Brainsight Primate; Rogue Research, Montreal, Canada). The injections were made through a 10-µl Hamilton Neuros Syringe (Hamilton, Reno, USA) at the rate of 0.2 µl/min (0.5 µl/site, two sites/track). The vector injections for eight tracks were performed in case of Monkey A and B, and those for twelve tracks were also performed in case of Monkey C and D. The tracks were placed at least 4.5 mm apart from each other, and no overlapping of adjacent injections was detected on any occasion, as also evidenced by the distribution gaps of transgene-expressing neurons. After the experiments, the monkeys were monitored until full recovery from the anesthesia.

All experimental procedures were performed in a special laboratory (biosafety level 2) designated for *in vivo* animal infectious experiments that had been installed at the Primate Research Institute, Kyoto University. Throughout the entire experiment, the

animals were kept in individual cages that were placed inside a special safety cabinet in controlled temperature (23-26°C) and light (12-hr on/off cycle) conditions. The animals were fed regularly with dietary pellets and had free access to water. Every effort was made to minimize animal suffering.

Chemogenetic manipulation

Under general anesthesia as described above, five distinct types of AAV vectors carrying the hM3Dq gene were injected bilaterally into the striatum (i.e., the caudate nucleus and putamen) in two monkeys (Monkeys E and F in Table 1). Stereotaxic coordinates of the injected sites were defined based on overlaid magnetic resonance (MR) and computed tomography (CT) images created by PMOD image analysis software (PMOD Technologies, Zurich, Switzerland). The injections were made through a 10-μl Hamilton microsyringe in a single needle penetration for each vector (3.0 μl/site, one site/track, at the rate of 0.5 μl/min). The tracks were placed at least 3.0 mm apart from each other, and no overlapping of adjacent injections was detected on any occasion, as also evidenced by the distribution gaps of transgene-expressing neurons. PET imaging was performed over a period of several months to one year using the procedures described previously[66]. Briefly, the monkeys were sedated with ketamine hydrochloride (5 mg/kg, i.m.) and xylazine hydrochloride (0.5 mg/kg, i.m.), and the anesthetized condition was maintained with isoflurane (1-2%, inhalation) during the PET imaging. PET scans were done with microPET Focus220 scanner (Siemens Medical Solutions, Malvern, USA). Following transmission scans, emission scans were acquired for 90 min after intravenous bolus injection of [^{11}C]DCZ (331.5-404.9 MBq) or [^{18}F]FDG (233.3-306.9 MBq). Pretreatment with DCZ (1 μg/kg; MedChemExpress, Monmouth Junction, USA) or vehicle (1-2%

dimethyl sulfoxide (DMSO) in 0.1-ml saline, without DCZ) was carried out 1 min before the [^{18}F]FDG injection. The PET imaging data were reconstructed with filtered back-projection with attenuation correction. Voxel values were converted to standardized uptake values (SUVs) that were normalized by injected radioactivity and body weight using PMOD. Volumes of interest (VOIs) were manually drawn on the center of the injection site and the cerebellum using PMOD, by referring to MR images of individual monkeys. To estimate the specific binding of [^{11}C]DCZ, the regional binding potential relative to nondisplaceable radioligand (BP$_{ND}$) was calculated with an original multilinear reference tissue model using the cerebellum as a reference region[67]. For FDG–PET analysis, dynamic SUV images were motion-corrected and then averaged between 60 and 90 min after the radioligand injection. The SUV ratio (SUVR) of voxel value was calculated as a percentage to the averaged value of the whole brain for comparison across the scans.

In vivo calcium imaging

In the remaining two monkeys (Monkeys G and H in Table 1), *in vivo* intrinsic signal optical imaging (ISOI), wide-field calcium imaging (WFCI) and two-photon calcium imaging (TPCI) of neurons in layers 2 and 3 of the V1 and V2 were performed. Under sterile conditions and isoflurane anesthesia (1-2%, inhalation), the cortical surface of V1 and V2 was exposed by incision of the scalp and removal of a skull portion and dura mater over these areas. The AAV2.1-A vector carrying the GCaMP6s gene was injected unilaterally into the V1 and V2 at six sites (1 μl at each site) in each monkey. For Monkey G, AAV2.1-A-CaMKIIα-GCaMP6s was injected into two loci at the titer of 2.0×10^{13} gc/ml. The same vector was injected into the other two sites at the titer of 1.0×10^{14} gc/ml.

In addition, AAV2.1-A-Syn-GCaMP6s was injected into two loci at the titer of 2.0×10^{13} or 1.0×10^{14} gc/ml. For Monkey H, AAV2.1-A-CaMKIIα-GCaMP6s was injected into six loci at the titer of 4.0×10^{13} gc/ml. The distance between the injection sites was at least 1.5 mm apart from each other. At each site, two injections were made at the depth of 1 and 2 mm (0.5 µl at each depth). After the vector injections, a chronic titanium imaging chamber (inner diameter, 12 mm) was implanted to cap the exposed cortex. The center of the chamber was positioned 15-mm lateral to the midline, and its anteroposterior position was adjusted so that the lunate sulcus ran along the one-third upper position of the chamber to allow a view of both V1 and V2[68]. The exposed cortex was covered with artificial dura (W. L. Gore & Associates, Inc., Newark, USA) that was glued to the chamber with silicone adhesive (Kwik-Sil; World Precision Instruments, Sarasota, USA) for preventing regenerative tissue from infiltrating into the imaging field[69]. The exposed cortex was further protected with a cover glass (Matsunami, Osaka, Japan; 14 mm in diameter and 0.5 mm in thickness), which was fixed to the chamber with a retaining ring (SM14RR; Thorlabs, Newton, USA). The retaining ring was glued to the titanium chamber with surgical silicone adhesive (Kwik-Sil).

When imaging experiments were performed, anesthesia was first introduced to the monkeys with ketamine and then maintained with propofol (induction, 5 mg/kg; maintenance, 5 mg/kg/hr, i.v.)[68]. The monkeys were paralyzed with vecuronium bromide (induction, 0.25 mg/kg, i.v.; maintenance, 0.05 mg/kg/hr, i.v.) and artificially respirated. The eyes were fitted with contact lenses of appropriate curvature to prevent from drying and focus on a stimulus screen 57-cm distant from the cornea[70,72].In ISOI, intrinsic signals were acquired by a CMOS camera tandem-lens setup (FLIR GS3-U3-41C6NIR-C; exposure time, 100-300 µs; aperture, f5.6; lens combination, Noct-Nikkor 58 mm for the

object side and Nikkor 50 mm for the CMOS side; Nikon, Tokyo, Japan) with 625-nm illumination (M625L3; Thorlabs) at a frame rate of 25 frames/s. One single imaging trial lasted 5 s (1 s before visual stimulus onset and 4 s after onset). The image size was 1024×1024 pixels representing a 12.5×12.5 mm^2 field of view, which covered the full field of the cortical surface within the imaging chamber. Images were acquired with custom-built software made with LabVIEW (National Instruments, Austin, USA). The setup for WFCI was similar to that for ISOI and shared the same imaging window and software. Calcium signals were acquired by the same CMOS camera (exposure time, 10-30 ms) through 500-nm-long pass filter (FELH0500; Thorlabs) under 490-nm illumination (M490L4; Thorlabs) at a frame rate of 25 frames/s. In TPCI, calcium signals were acquired with a two-photon excitation microscope (MOM with 8 kHz resonant scanner; Sutter, Novato, USA) equipped with a 16×, NA 0.8 water immersion objective lens (CFI175-LWD-16XW; Nikon) and 920-nm excitation laser (Insight X3; Spectra Physics, Milpitas, USA). The frame rate was 30.9 frames/s. The size of image areas was 512×512 pixels representing a 630×630 μm^2 field of view.

Visual stimuli were created using ViSaGe Mk II (Cambridge Research Systems, Rochester, UK) and displayed on a gamma-calibrated 23-inch LCD monitor (MDT231WG; Mitsubishi Electronic, Tokyo, Japan). Full-screen drifting black-white square-wave gratings were presented. The duty cycle of gratings was 0.2 (20% white), and the spatial frequency was 1.5 cycle/degree. The gratings drifted at 8°/s and were presented in a randomly interleaved fashion in four orientations (0°, 45°, 90°, and 135°) with two opposite moving directions (i.e., eight directions; 0°, 45°, 90°, 135°, 180°, 225°, 270°, and 315°). Adding a blank screen condition, there were nine stimulus conditions in

total. Each stimulus condition lasted 4 s. The initial phase of the gratings was randomly selected.

In data analysis, the magnitude of fluorescence response ($\Delta F/F$) was first quantified using the following formula: $\Delta F_i/F = (F_i - F_0)/F_0$, in which F_i was a response in an *i*-th single frame after stimulus onset, and F_0 was an averaged response of frames over a period of 1 s before stimulus onset. This fluorescence response was used to describe the response time course of a population of single neurons. In ISOI and WFCI, responses to orthogonal orientations by performing subtraction of the averaged $\Delta F/F$ between two orthogonal orientation conditions was compared. For this analysis, responses to opposite directions with the same orientation gratings were averaged. All image processing procedures were done with the MATLAB (Mathworks). Blood vessel mask was created based on the cortical image under 530-nm illumination (M530L3; Thorlabs).

Histology and image acquisition

The six monkeys (Monkeys A-F) underwent perfusion-fixation. The approximate survival periods after the vector injections were four weeks for Monkeys A-D, over six months for Monkey E, over 12 months for Monkey F, and three weeks for the rats. In Monkeys E and F, DCZ was administered systemically 2 hr prior to sacrifice for analysis of c-fos expression. The animals were anesthetized deeply with an overdose of sodium pentobarbital (50 mg/kg, i.v.) and perfused transcardially with 0.1 M PBS, followed by 10% formalin in 0.1 M phosphate buffer. The removed brains were postfixed in the same fresh fixative overnight at 4°C and saturated with 30% sucrose in 0.1 M PBS at 4°C. Coronal sections were cut serially at the 50-µm thickness on a freezing microtome and grouped into ten series. Every tenth section was used for individual histological analyses.

Double fluorescence histochemistry for NeuN and S100β was performed for Monkeys A-D. Briefly, coronal sections were incubated with a cocktail of guinea pig polyclonal antibody against NeuN (1:1,000; Millipore) and mouse monoclonal antibody against S100β (1:5,000; Sigma-Aldrich). These sections were then incubated with a cocktail of DyLight 405-conjugated donkey anti-guinea pig IgG antibody and Alexa 647-conjugated donkey anti-mouse IgG antibody (1:200; Jackson ImmunoResearch, West Grove, USA). For Monkeys E and F, double immunofluorescence histochemistry for GFP and DARPP-32, PV, or ChAT was performed. Coronal sections were incubated with chicken monoclonal antibody against GFP (1:2,500; Abcam, Cambridge, UK) and rabbit monoclonal antibody against DARPP-32 (1:250; Cell Signaling Technology, Danvers, USA), mouse monoclonal antibody against PV (1:2,000; Sigma-Aldrich), or goat monoclonal antibody against ChAT (1:200; Sigma-Aldrich). These sections were then incubated with Alexa 488-conjugated donkey anti-chicken IgG antibody (1:400; Jackson ImmunoResearch) and Alexa 555-conjugated donkey anti-rabbit antibody (1:400; Invitrogen), Alexa 555-conjugated donkey anti-mouse IgG antibody (1:400; Invitrogen), or Alexa 647-conjugated donkey anti-goat IgG antibody (1:400; Jackson ImmunoResearch).

For immunohistochemical staining for GFP, hM3Dq, and c-fos following chemogenetic manipulation, coronal sections were pretreated with 0.3% H_2O_2 for 30 min, rinsed three times in 0.1 M PBS, and immersed in 1% skim milk for 1 hr. The sections were then incubated for two days at 4°C with rabbit monoclonal anti-GFP antibody (1:2,000; Invitrogen, Waltham, USA), rabbit polyclonal anti-M3 (muscarinic acetylcholine receptor M3) antibody (1:200; Atlas Antibodies, Stockholm, Sweden), or rabbit polyclonal anti-c-fos antibody (1:2,000; Abcam) in 0.1 M PBS containing 2%

normal donkey serum and 0.1% Triton X-100. Subsequently, the sections were incubated with biotinylated donkey anti-rabbit IgG antibody (1:1,000; Jackson ImmunoResearch) in the same fresh medium for 2 hr at room temperature, followed by the avidin-biotin-peroxidase complex (ABC *Elite*; 1:200; Vector laboratories, Burlingame, USA) in 0.1 M PBS for 2 hr at room temperature. The sections were finally reacted for 10-20 min in 0.05 M Tris-HCl buffer (pH 7.6) containing 0.04% diaminobenzine tetrahydrochloride (Wako, Osaka, Japan), 0.04% $NiCl_2$, and 0.002% H_2O_2. The reaction time was set to make the density of background immunostaining almost identical across different sections. All histological sections were mounted onto gelatin-coated glass slides and counterstained with 0.5% Neutral red.

A high sensitivity charge-coupled device (CCD) camera (VB-7010, Keyence, Osaka, Japan) was used to capture bright-field and fluorescence images from the whole brain sample. To capture the bright-field and fluorescence images in coronal sections, a scientific CMOS (sCMOS) camera (In Cell Analyzer 2200; GE Healthcare, Chicago, USA) was used. Merged images of mKO1 and NeuN/GFAP-immunofluorescent coronal sections were created by using Fiji/ImageJ software[72]. A confocal laser-scanning microscope (LSM800; Carl Zeiss, Oberkochen, Germany) was also used to take fluorescence images. Merged images were prepared by using the Zeiss Zen 3.3 software (Carl Zeiss).

Intensity analysis of mKO1 native-fluorescence at injection sites

The intensity of mKO1 native-fluorescence emitted from each vector injection site was measured in sections of the monkey brains by using MATLAB software (Mathworks, Natick, USA). The region for measurement in each section was determined according to

the highest one selected from the averaged intensity values within circular observation windows (2-mm diameter). Three sections were chosen including the sections through the center of the injection site (revealed by the highest fluorescence intensity) and 500 μm anterior/posterior to the injection site. In each case, intensity measurement at the injection site was performed by setting circles with the highest intensity, and the averaged value of fluorescence intensity obtained in the three sections was calculated to determine the relative transgene expression level for each vector. To estimate the transgene expression level at each injection site, the expression level for the AAV2-CMV or AAV5-CMV vector was defined as 1.0, and the relative value to this was calculated for the other vectors.

Neuron specificity analysis of transgene-expressing cells at injection sites

The number of RFP-positive cells expressing NeuN or S100β was counted at the injection sites of the vectors in Monkeys A-D. Three sections were chosen in the same fashion as described above. Stereological cell counts assisted with Stereo Investigator software (MBF Biosciences, Williston, USA) were carried out in 100×100 μm^2 counting frames equally spaced across a grid of 250×250 μm^2 (monkeys) or 150×150 μm^2 (rats) with an 18-μm-high optical dissector (average section thickness, 25 μm for monkeys, 20 μm for rats). The cell counts were done over the whole transgene-expressing region in each section. Based on these data, the ratio of double-labeled cells to the total RFP-positive cells was calculated.

Counts of mKO1- and c-fos-positive neurons

For counts of mKO1-positive neurons at the cortical injection sites, three sections were selected in the same manner as described above. The number of mKO1-positive neurons was counted by the aid of Stereo Investigator software (MBF Biosciences). For counts of c-fos-positive neurons in the striatum, Neurolucida software (MBF Biosciences) was used to set circular observation windows with the densest labeling (1-mm diameter), and the averaged value of cell counts was calculated.

2.3. Results

Production of mosaic AAV vectors

Two types of mosaic AAV vectors with different ratios of AAV1 and AAV2 capsid proteins were produced: AAV2.1-A vector with a combined capsid of 10% AAV1 capsid protein and 90% AAV2 capsid protein, and AAV2.1-B vector with a combined capsid of 50% AAV1 capsid protein and 50% AAV2 capsid protein. According to previous *in vitro* studies[46,47,65], the AAV2.1-B vector was initially made. In the preliminary survey, however, it was found that a certain degree of glial infectivity remained in this vector. Therefore, the AAV2.1-A vector was developed with a significant reduction (10%) in the ratio of AAV1 capsid protein. A total of 14 different kinds of vectors based on the AAV2, AAV1, and their mosaic vectors was produced for three sets of our experiments (Table 1): morphological analysis of gene transduction properties (Monkeys A-D), chemogenetic modulation of neuronal activities (Monkeys E and F), and *in vivo* calcium imaging of neuronal activities (Monkeys G and H). The production efficiency (stock titer) of each vector is listed in Table 1. In general, AAV2 vectors had a lower efficiency than AAV2.1 and AAV1 vectors.

Gene transduction properties of mosaic AAV vectors

First, I investigated gene transduction properties of the mosaic AAV2.1-A and AAV2.1-B vectors by comparing with those of the original AAV2 and AAV1 vectors. Two types of promoters, ubiquitous cytomegalovirus (CMV) promoter and neuron-specific synapsin (Syn) promoter, were utilized for evaluating the neuron specificity of the vectors and analyzing their transgene expression levels within neurons, respectively. I injected the following eight distinct kinds of AAV vectors carrying the mKO1 gene into the medial

wall of the frontal lobe (involving areas 4, 6, and 9) in two macaque monkeys (Monkeys A and B in Table 1): the AAV-CMV-mKO1 vectors decorated with four different compositions of capsids (AAV2, AAV2.1-A, AAV2.1-B, and AAV1) and the AAV-Syn-mKO1 vectors with the same virions (Fig. 1a). All vectors inserted with CMV promoter were injected at the titer of $1.5×10^{13}$ genome copies (gc)/ml, while those inserted with Syn promoter were at the titer of $6.0×10^{13}$ gc/ml to make the transgene expression for the AAV2 vector detectable. The tracks of cortical injections were placed at least 4.5 mm apart from each other, and no marked overlapping of adjacent injections was detected, as also evidenced by the distribution gaps of transgene-expressing neurons.

I compared the intensity of transgene expression among these vectors at their cortical injection sites (Fig. 1b). The transgene expression level was first quantified as an averaged value of the red fluorescent protein (RFP) signal within a circle of 2.0-mm diameter and normalized to the expression level for the AAV2-CMV vector which was defined as 1.0 (Fig. 1c). Concerning the vectors inserted with CMV promoter, both the AAV1 and the AAV2.1-B vectors exhibited somewhat higher levels of transgene expression than the AAV2.1-A vector. With respect to the vectors inserted with Syn promoter, the AAV2.1-A vector displayed the highest expression level among these three vectors. Regardless of the promoter type, the transgene expression levels for the AAV2 vectors were lower than the others; the expression level was only less than half or one-fifth of that for the AAV2.1-A vector (Fig. 1c). I then quantified the number of cortical neurons (NeuN-positive; see below) expressing the transgene at the sites of vector injections (Fig. 1d). Our cell counts using stereology revealed that, irrespective of the promoter type, the AAV2.1-A or AAV2 vector yielded the largest or smallest number of RFP-positive neurons, respectively. The numbers of RFP-positive neurons transduced via the AAV2.1-B and AAV1 vectors were

in between. Thus, data obtained from the fluorescence intensity analysis of the vectors inserted with Syn promoter corresponded closely to those from the cell-count analysis for both CMV and Syn promoters (compare Fig. 1c with Fig. 1d), indicating that the AAV2.1-A vector produced a higher level of gene transduction into neurons compared with the other vectors.

Subsequently, I examined the neuron specificity of the mosaic vectors in comparison with the original vectors. Fluorescence histochemistry was applied to analyze colocalization of NeuN as a neuronal marker or S100β as an astroglial marker in RFP-positive cortical cells (Fig. 2a; Monkeys A and B in Table 1). Cell counts were done by means of the stereological method, and the ratio of double-labeled cells to the total RFP-positive cells was calculated. Data on the vectors with ubiquitous CMV promoter showed that the neuron specificity of the AAV2.1-A vector was high enough to reach the level of the AAV2 vector, while the AAV2.1-B vector had certain glial infectivity, the extent of which was close to that of the AAV1 vector (Fig. 2b). The vectors with Syn promoter exhibited almost complete levels of neuron-specific gene expression, except that a trace of transgene expression in S100β-positive cells remained for the AAV1 vector (Fig. 2b). Overall, among the four vectors tested here, the AAV2.1-A vector possessed the capability of most efficient and neuron-specific expression of the transgene. It should be noted that given their glial infectivity, the transgene expression levels for the AAV1 and AAV2.1-B vectors with CMV promoter, which were more intense than that for the AAV2.1-A vector, might have represented the signal issued not only from neurons, but also from glial cells.

I further compared the gene transduction properties of the AAV2.1-A vector with those of the AAV5 and AAV9 vectors (see Table 1), both of which have often been used in previous studies on rodent as well as primate brains[30,34,35,57,73-75]. The AAV-CMV-

mKO1 vectors decorated with four different compositions of capsids (AAV2.1-A, AAV1, AAV5, and AAV9) and the AAV-Syn-mKO1 vectors with the same virions were injected into the medial frontal cortex of two monkeys (Monkeys C and D in Table 1; Fig. 3a,b). As in the experiments described above, the vectors were injected at the titer of 1.5×10^{13} gc/ml (for CMV promoter) or 6.0×10^{13} gc/ml (for Syn promoter). To account for the possibility that the infection property of the vectors differs among cortical areas, AAV2.1-A vectors were injected at three loci of the medial frontal cortex, and AAV1, 5, and 9 vectors were injected almost symmetrically on the side contralateral to each of the AAV2.1-A vector injection sites (Fig.3a). The transgene expression level was quantified in the same fashion as in the above experiments and normalized to the expression level for the AAV5-CMV vector which was defined as 1.0 (Fig. 3c). It was found that each AAV2.1-A vector injection yielded similar results on both RFP expression level and RFP-positive neuron number, indicating that the vector infection efficiency was stable, at least within the frontal cortex. Among the vectors inserted with CMV promoter, the AAV9 vector displayed the greatest capacity in both the RFP expression level and the RFP-positive neuron number, followed by the AAV2.1-A and AAV1 vectors (Fig. 3c,d). Among the vectors inserted with Syn promoter, on the other hand, the AAV2.1-A vector exhibited the capacity of gene transduction as high as the AAV9 vector. Regardless of the promoter type, the gene transduction capacity of the AAV5 vector was lower than the others. Data obtained from the fluorescence intensity analysis of the vectors inserted with Syn promoter were in close register with those from the cell-count analysis using both CMV and Syn promoters (compare Fig. 3c with Fig. 3d).

I then analyzed the neuron specificity of the AAV5 and AAV9 vectors in comparison with the AAV2.1-A and AAV1 vectors. Fluorescence histochemistry was performed to

32

examine colocalization of NeuN or S100β in RFP-positive cortical cells (Fig. 4a). Data on the vectors with CMV promoter revealed that not only the AAV1 vector (see also Fig. 2), but also the AAV5 and AAV9 vectors exhibited distinct levels of glial infectivity, whereas the AAV2.1-A vector displayed the highest level of neuron specificity (Fig. 4b). Such high neuron specificity of the AAV2.1-A vector was consistent across the frontal cortical areas tested. The vectors with Syn promoter had almost perfect neuron-specific gene transduction, except that transgene expression in S100β-positive cells slightly remained for the AAV9 vector (Fig. 4b). Thus, the level of transgene expression especially for the AAV9 vector with CMV promoter, which was apparently more intense than that for the AAV2.1-A vector, might have represented the signal emitted from glial cells as well as from neurons.

Application of AAV2.1-A vector to chemogenetic manipulation

Second, the usefulness of the AAV2.1-A-Syn vector in chemogenetic manipulation of neuronal activity in the primate brain was explored, by applying a recombinant vector carrying the modified human M3 muscarinic receptor (hM3Dq) gene to the excitatory DREADDs (designer receptors exclusively activated by designer drugs) system[9]. The IRES-GFP (green fluorescent protein) sequence was further inserted as a fluorescent protein tag to examine properties of transduced neurons (AAV2.1-A-Syn-hM3Dq-IRES-GFP; Table 1). For comparison, four different vectors carrying the hM3Dq gene which were based on the original AAV2 or AAV1 vector and inserted with Syn or CMV promoter were prepared (AAV2-Syn-hM3Dq-IRES-GFP, AAV2-CMV-hM3Dq-IRES-GFP, AAV2-Syn-hM3Dq, and AAV1-Syn-hM3Dq-IRES-GFP; Table 1). These vectors were tested in terms of the potential of receptor binding, the responsiveness to ligand administration,

and the duration of transgene expression. They were injected into the striatum, the caudate nucleus or putamen, of each hemisphere in two macaque monkeys (Monkeys E and F in Table 1; Figs. 2-5a,e and 2-6a,b).

In the first monkey (Monkey E), the comparison of the AAV2.1-A vector with the AAV2 vector in terms of the three aspects listed above were performed. Three types of highly neuron-specific vectors were injected into the striatum: the AAV2.1-A-Syn vector into the caudate nucleus and putamen on one side, and the AAV2-CMV vector into the caudate nucleus and the AAV2-Syn vector into the putamen on the other side (Fig. 2-5a; see also Fig. 2-6a). The injection titer of these vectors was set at 1.0×10^{13} gc/ml, except that the AAV2.1-A-Syn vector was additionally injected at 5.0×10^{13} gc/ml into the putamen since its production efficiency (stock titer) was higher than those of the AAV2-CMV/Syn vectors (Table 1). To evaluate the potential of DREADDs receptor binding *in vivo*, relevant to the strength of hM3Dq expression, positron emission tomography (PET) imaging with radiolabeled deschloroclozapine ($[^{11}C]$DCZ) was carried out (see ref. 66). To monitor the time-dependent changes in hM3Dq expression, $[^{11}C]$DCZ-PET scans were performed in the monkey at four times (30, 45, 80, and 184 days) post-injection (Fig. 2-5b,c). To verify the responsiveness to DREADDs ligand administration, an attempt was made to chemogenetically activate neurons where hM3Dq was expressed through the AAV vectors. PET imaging with radiolabeled fluorodeoxyglucose ($[^{18}F]$FDG) was used for *in vivo* visualization of glucose metabolism as an index of neuronal/synaptic activation[76-78]. To detect the FDG uptake following systemic administration of DCZ, $[^{18}F]$FDG-PET scans were performed in the monkey at twice (86 and 193 days) after the vector injections (Fig. 2-5d; see also ref. 66).

When the vectors were injected at the titer of 1.0×10^{13} gc/ml, the AAV2.1-A vector exhibited a high level of $[^{11}C]$DCZ binding (hM3Dq expression; see ref. 33), whereas the $[^{11}C]$DCZ binding levels for the AAV2 vectors were quite low regardless of the promoter type (Fig. 2-5b,c). In addition, the AAV2.1-A vector injected at a higher titer $(5.0 \times 10^{13}$ gc/ml) displayed an even greater level of $[^{11}C]$DCZ binding compared with the lower-titer one (Fig. 2-5b,c). The $[^{11}C]$DCZ-PET scans showed that the extent of $[^{11}C]$DCZ binding for the AAV2.1-A vector was gradually increased until 45 days post-injection and then appeared to reach the plateau. Such hM3Dq expression lasted over six months (Fig. 2-5b,c). Similar results were obtained from the $[^{18}F]$FDG-PET scans. At the injection site of the AAV2.1-A vector at the lower as well as the higher titer, the extent of FDG uptake was markedly increased by DCZ administration at 86 days after the vector injection and retained even at 193 days post-injection (Fig. 2-5d). By contrast, virtually no increase was found for either type of the AAV2 vectors (Fig. 2-5d).

In the second monkey (Monkey F), four types of vectors were injected into the striatum: the AAV2-Syn vector into the caudate nucleus and the AAV2.1-A-Syn vector into the putamen on one side, and the AAV2-Syn vector without GFP tag into the caudate nucleus and the AAV1-Syn vector into the putamen on the opposite side (Fig. 2-5e; see also Fig. 2-6b). The injection titer of these vectors was set at 2.0×10^{13} gc/ml. Since the AAV2 vector without fluorescent protein tag and the AAV1 vector have been used in previous DREADDs studies in which animal behavior was successfully manipulated[33,66], the validity of the AAV2.1-A vector was analyzed in comparison with these conventional vectors. In this monkey, $[^{11}C]$DCZ-PET scans were carried out at seven times (30, 45, 64, 120, 143, 176, and 358 days) after the vector injections. Similar high levels of $[^{11}C]$DCZ binding (hM3Dq expression) were observed for all of the AAV2 vector without GFP tag,

35

the AAV1 vector, and the AAV2.1-A vector (Fig. 2-5f,g). The binding levels were gradually increased until 64 days post-injection and then reached the plateau. Such hM3Dq expression was retained as long as one year (Fig. 2-5f,g). With respect to the FDG uptake, [^{18}F]FDG-PET scans were performed at five times (49, 72, 129, 182, and 365 days) after the vector injections and observed that the AAV2.1-A vector, together with the AAV2 vector without GFP tag and the AAV1 vector, displayed a high level of FDG uptake induced by DCZ administration (Fig. 2-5h). Such responsiveness of striatal neurons to the DREADDs ligand also lasted over one year. The FDG uptake for the AAV2 vector without GFP tag seemed higher than the AAV2.1-A and AAV1 vectors. Consistent with the findings obtained in the first monkey, the AAV2-Syn vector with GFP tag exhibited much lower levels of [^{11}C]DCZ binding and FDG uptake than the other three vectors (Fig. 2-5h).

I histologically confirmed the PET imaging data described above. The immunohistochemical analysis with anti-GFP or anti-muscarinic acetylcholine receptor M3 (M3) antibody demonstrated that the sites of hM3Dq expression visualized by [^{11}C]DCZ-PET imaging corresponded to GFP-positive regions in the striatum (Fig. 2-6a,b). To verify neuronal activation chemogenetically induced by DCZ administration 2 hr before sacrifice, the density of striatal neurons expressing c-fos was examined at the injection site of each vector (Fig. 2-6c,d). Consistent with the findings obtained from [^{18}F]FDG-PET imaging, a large number of c-fos-expressing neurons were found after DCZ administration at the striatal injection sites of the AAV2.1-A vector including the higher-titer one, as compared to the AAV2 vector with GFP tag (Fig. 2-6c-f). On the other hand, striatal neurons expressing c-fos were more frequently seen at the injection sites of the AAV2 vector without GFP tag and the AAV1 vector (Fig. 2-6d,f). Our GFP

immunohistochemical observations revealed that axon terminal labeling from the striatal injection site was evident in the substantia nigra (pars reticulata), whereas only very rarely was found cell body labeling in the substantia nigra (pars compacta), thalamus, or cerebral cortex, all of which are known to send projection fibers to the striatum (Fig. 2-6g). This indicates that the AAV2.1-A vector was preferentially taken up from cell bodies and dendrites, but not from axon terminals.

I characterized striatal neurons in which the transgene was expressed via the AAV2.1-A vector by identifying their neuron types (i.e., projection neurons vs. interneurons). Fluorescence histochemistry was performed to analyze colocalization of dopamine- and cAMP-regulated phosphoprotein (DARPP-32) as a medium spiny projection neuron marker, or parvalbumin (PV)/choline acetyltransferase (ChAT) as fast-spiking/cholinergic interneuron markers in GFP-positive cells. It was found that the AAV2.1-A vector was transduced into both projection neurons and interneurons in the striatum (Fig. 2-7).

Application of AAV2.1-A vector to in vivo calcium imaging

Third, applicability of the AAV2.1-A vector to *in vivo* calcium imaging of neuronal activities was investigated in the primate cerebral cortex. A recombinant vector expressing GCaMP6s was produced and injected it into the primary and secondary visual cortical areas (V1 and V2) of two macaque monkeys (Monkeys G and H in Table 1).

First, intrinsic signal optical imaging was performed to visualize orientation maps of V1 and V2 by examining response signals to drifting gratings of various orientations. One-photon wide-field calcium imaging and two-photon calcium imaging carried out to capture fluorescence signals from neurons in V1 (Fig. 2-8a for Monkey H; Fig. 2-9a for

Monkey G). In both monkeys, V1 neurons loaded with the recombinant DNA exhibited fluorescence responses time-locked to visual stimulation. The responses of were pronounced, exhibiting $\Delta F/F$ as high as 400 % in some neurons (Fig. 2-8b,c). They were selective to a particular range of orientation of gratings (Fig. 2-8c). The orientation selectivity of imaged neurons was consistent with that determined by intrinsic optical signal recording and by one-photon wide-field calcium imaging (Fig. 2-8a). Repeated imaging showed that the fluorescence signals could be recorded over eight months after the vector injection. Even at 244 days post-injection, the captured signals were comparable to those at 41 days post-injection in Monkey H (Fig. 2-8b). Intrinsic signal optical imaging revealed stable orientation maps without any unresponsive local regions over this prolonged experimental period, indicating that the viral injection did not cause noticeable damage in the cortex. The results demonstrate that the mosaic vector developed in the present study provides a sensitive, reliable, and stable tool to monitor neuronal activities in the primate cerebral cortex.

2.3. Discussion

In the present study, the mosaic AAV vector, termed AAV2.1 vector, of which capsid was composed of capsid proteins derived from both AAV1 and AAV2 was newly developed. Of the two types of mosaic vectors with different compositions of their capsid proteins, the AAV2.1-A vector of which capsid was obtained from a higher ratio of AAV2 capsid protein (10% AAV1 and 90% AAV2) has successfully met the two requirements, high levels of transgene expression and neuron specificity. Our analysis in the monkey cerebral cortex has revealed that this vector possesses the excellence in transgene expression (for the AAV1 vector) and neuron specificity (for the AAV2 vector) simultaneously (see Figs. 2-1 and 2-2). It should be noted that similar AAV vectors, decorated with a mosaic capsid consisting of AAV1 and AAV2 capsid proteins, showed enhanced levels of transgene expression in the muscle and liver in mice[46]. In this previous study, a mosaic vector obtained from the same ratio of both capsid proteins, equivalent to our AAV2.1-B vector, has the advantage of gene transduction over those from their different ratios[46]. Although such a discrepancy may be ascribable to the differences in target organs and/or animal species, the composition of capsid proteins is certainly responsible for gene transduction properties of the vectors. Among the vectors inserted with CMV promoter, the intensity of transgene expression for the AAV2.1-A vector was lower than those for the AAV1 vector and the AAV2.1-B vector. When the CMV promoter was replaced with the Syn promoter, however, the AAV2.1-A vector exhibited the highest level of transgene expression. In view of the fact that the AAV1 and AAV2.1-B vectors with CMV promoter displayed some extent of glial infection, the intensity of their transgene expression might have represented signals derived from both neurons and glial cells. Conversely, transgene expression in neurons via these vectors were limited under

the control of Syn promoter. The data obtained from the fluorescence intensity analysis of the vectors with Syn promoter corresponded closely to those from the cell-count analysis using both CMV and Syn promoters. This implies that differential transgene expression levels for the vectors inserted with Syn promoter reflect the difference in the number of transgene-expressing neurons, albeit distinct expression levels within individual neurons cannot as yet be excluded.

Although the transgene expression efficiency and neuron specificity of the AAV2.1 vector were stable in the medial frontal cortex of the monkey, it should be noted here that this result was obtained from the comparison of many serotypes of AAV vectors injected into distinct cortical areas of four monkeys. In the monkey experiments, it is quite difficult to minimize a bias caused by the individual differences, unlike the rodent experiments which are easy to make subjects' properties uniform, such as genetic background, sex, age, and weight. Therefore, it is not so realistic as to compare statistically the properties of numbers of vectors in the monkey brain under the same conditions. In our study, the highest number of neurons were transduced at the site of each vector injection in Monkey A whose age was 18 years old. On the other hand, the number of transduced neurons was fewer and similar in Monkeys B-D who were relatively close in age (Monkey B, 11 years old; Monkey C, 8 years old; Monkey D, 12 years old). Although the age of subjects may have affected the transgene expression efficiency or neuron specificity of the AAV vectors, the present results were stable when the levels of transgene expression were compared in the AAV2.1-A vector and the other serotype vectors which were injected in single monkeys. Furthermore, it was found that higher neuron specificity (i.e., lower glial infectivity) of the AAV2.1-A vector than that of the AAV1, 5, and 9 vectors were stable among the monkeys.

Moreover, the AAV2.1-A vectors expressing excitatory DREADDs and GCaMP have successfully been applied to chemogenetic manipulation and *in vivo* calcium imaging, respectively, in the primate brain (see Figs. 2-5, 6, 8, and 9). These AAV2.1-A vectors secured intense and stable expression of the target protein to achieve unequivocal modulation and imaging of neuronal activities. The overall data in our chemogenetic manipulation experiments have demonstrated that the AAV2.1-A vector displayed high levels of both the potential of DREADDs receptor binding and the responsiveness to DREADDs ligand administration. It should also be mentioned that the AAV2.1-A vector employed at a higher titer yielded a greater capacity of transgene expression (see Table 1). The transgene expression capacity of the AAV2 vector was lower regardless of the promoter type even compared with the AAV2.1-A vector at the same titer. In striking contrast, the capacity of the AAV2 vector without fluorescent protein tag became much higher, especially in terms of the responsiveness to DREADDs ligand administration. It is generally accepted that insertion of the IRES-GFP sequence into conventional AAV vectors dampens transgene expression[79-81]. However, given its potentially high level of transgene expression, the AAV2.1-A vector can be considered to retain a sufficient expression level even with the fluorescent protein tag inserted. While other non-fluorescent tag proteins are available, AAV vectors expressing no marker proteins within either somas or nuclei do not likely merit application to anatomical studies which require histological determination of the localization, number, and/or type of transduced cells.

The AAV2.1-A has accomplished both the high-level target gene expression in neuronal cells and the minimal infection to glial cells. To achieve the high-yield transgene expression in the primate brain, the AAV1, AAV5, and AAV9 vectors have often been utilized[13,25,30,34,35,57]. In the present study, the glial as well as neuronal

infectivity was detected in the AAV1, 5, and 9 vectors (see Figs. 2-3 and 4). For the AAV1, 5, and 9 vectors to secure neuron-specific gene expression, the selection of a promoter, like Syn promoter, is therefore critical. However, even though the Syn promoter restricts the cell type to neurons in which the transgene is expressed via the vectors, it is still impossible to avoid infection to non-neuronal cells (i.e., glial cells) with these serotypes per se, and transgene expression due to leaky Syn promoter activity or ITR promoter activity may occur as I observed in the case of AAV1- and AAV9-Syn-mKO1 vector injections into the monkey cortex[82]. Such viral infection to and transgene expression in glial cells may cause inflammatory changes in the brain. Indeed, it has been reported that the conventional serotypes of AAV vectors, especially the AAV9 vector, induce inflammatory responses due to the glial transduction[13,14,37-39,60,83]. Presumable tissue damage caused by the inflammatory responses discourages their application to long-term experiments over years in primates. Thus, the AAV2.1-A permits behavioral and electrophysiological monitoring over a long time period by a potential reduction in inflammatory responses.

For recent years, many neuroscientists have made an effort to achieve reliable and stable modulation of neuronal activity and animal behavior by combining the viral vector system with various cutting-edge techniques. The AAV2.1-A vector developed in the present study bears a prominent advantage over the conventional AAV vectors in view of both transgene expression and neuron specificity in the primate brain. Such a mosaic AAV vector can be a versatile tool for diverse *in vivo* approaches, including chemogenetic manipulation and *in vivo* calcium imaging. The AAV2.1-A vector exhibited excellent neurotropism even without Syn promoter. This enables us to replace the Syn promoter with other types of promoters so as to modify the transgene expression pattern or achieve

the neuron type-selective gene transduction. The widespread and effective application of the AAV2.1-A vector not only could facilitate elucidating neural network mechanisms underlying various brain functions, but also might subserve development valid primate models of neurological/psychiatric disorders.

Chapter 3: General Discussion

3.1. Summary of results

In Chapter 2, the comparison of the properties between the AAV2.1 vector and several conventional AAV vectors in the primate brain was performed as the first series of experiments. The novel mosaic AAV vector of which capsid was composed of capsid proteins derived from both of the AAV serotypes 1 and 2 (AAV1 and AAV2) was developed. Two types of mosaic AAV vectors with different ratios of AAV1 and AAV2 capsid proteins were produced: AAV2.1-A vector with a combined capsid of 10% AAV1 capsid protein and 90% AAV2 capsid protein, and AAV2.1-B vector with a combined capsid of 50% AAV1 capsid protein and 50% AAV2 capsid protein. I investigated gene transduction properties of the mosaic AAV2.1-A and AAV2.1-B vectors by comparing with those of the original AAV2 and AAV1 vectors. To compare the gene transduction efficiency in neurons, I examined the fluorescent intensity and the number of fluorescent protein positive neurons transduced via the AAV2.1-A, AAV2.1-B, AAV1, and AAV2 vector with neuron-specific synapsin (Syn) promoter at their cortical injection sites. I found that the AAV2.1-A vector displayed the highest transgene expression level among four vectors (Fig. 2-1). Subsequently, the neuron specificity of the mosaic vectors in comparison with the original vectors was examined. Although the AAV2 and AAV2.1-A vector showed almost complete levels of neuron-specific gene expression, the AAV1 and AAV2.1-B exhibited certain glial infectivity (Fig. 2-2). In conclusion, the AAV2.1-A vector successfully achieved both high levels of transgene expression and neuron specificity.

To confirm whether the AAV2.1 vector have superiority to the other conventional AAV vectors, I further compared the gene transduction properties of the AAV2.1-A

vector with those of the AAV5 and AAV9 vectors which have often been utilized in previous studies on primate brains[30,34,35,57,73-75]. Among the vectors inserted with neuron-specific Syn promoter, the AAV2.1-A vector exhibited high levels of transgene expression as high as that of the AAV9 vector (Fig. 2-3). The gene transduction capacity of the AAV5 vector was lower than the others. The neuron specificity of the AAV5 and AAV9 vectors was also analyzed and it was found that the AAV5 and AAV9 vectors exhibited distinct levels of glial infectivity, whereas the AAV2.1-A vector displayed the highest level of neuron specificity (Fig. 2-4). In conclusion, it was indicated that the AAV2.1-A vector has equivalent or higher levels of transgene expression to that of the AAV9 and AAV5 vector without glial infectivity.

Second, the utility of the AAV2.1-A-Syn vector in chemogenetic manipulation of neuronal activity in the striatum of primate brains was explored, by applying a recombinant vector carrying the hM3Dq gene to the excitatory DREADDs system. By using the PET imaging with radiolabeled deschloroclozapine ($[^{11}C]$DCZ) and radiolabeled fluorodeoxyglucose ($[^{18}F]$FDG), the visualization of expression levels of DREADD receptors and glucose metabolism as an index of neuronal/synaptic activation was achieved *in vivo*. These experiment yields that the AAV2.1-A vector exhibited a high level of $[^{11}C]$DCZ binding (hM3Dq expression) and $[^{18}F]$FDG uptake compared to that of the AAV2 vector (Fig. 2-5). It was observed that the transgene expression of the AAV2.1-A vector was lasted for 1 year and the neuronal activity was also successfully manipulated. The histological analysis of injection sites also supported these results (Fig. 2-6).

Third, it was investigated that the applicability of the AAV2.1-A vector to *in vivo* calcium imaging of neuronal activities in the primate cerebral cortex. A recombinant

vector expressing GCaMP6s was produced and injected into the primary and secondary visual cortical areas (V1 and V2) of two macaque monkeys. One-photon wide-field calcium imaging and two-photon calcium imaging was performed to visualize neuronal activity in V1 and V2 by examining the fluorescence signals emitted by neurons in response to visual stimuli of various orientations. Repeated calcium imaging showed that the fluorescence signals were successfully recorded over eight months after the vector injection (Fig. 2-7). Furthermore, prior to calcium imaging, intrinsic signal optical imaging (ISOI) was also conducted in the visual cortex to capture the changes in blood volume/oxidation resulting from neural activity in response to visual stimuli. According to the results of ISOI, any unresponsive local regions were not captured over eight months after vector injection. This indicates that the AAV2.1 vector did not cause damage in infected neurons over the prolonged experimental period due to its low inflammatory properties. In conclusion, it was indicated that the AAV2.1 vector expressing GCaMP6s has an optimal property for neuronal activity imaging in primate brains, stable and prolonged neuronal activity.

The AAV2.1 vector developed in the present study has a prominent advantage over the conventional AAV vectors in view of both transgene expression and neuron specificity in the primate brain. Such a mosaic AAV vector can be a versatile tool for diverse *in vivo* approaches, including chemogenetic manipulation and *in vivo* calcium imaging. The broad and efficient applications of the AAV2.1-A vector could not only aid in uncovering the neural network mechanisms that underlie various brain functions, but also contribute to the establishments of valid animal models in primates for studying neurological and psychiatric disorders.

3.2. Possibility of mosaic AAV vector acquiring characteristics from original AAV

vectors

A mosaic AAV vectors which has two superior characteristics of original AAV vectors was successfully developed. Previous studies were performed to develop such a mosaic AAV vectors. Rabinowitz et al. developed mosaic AAV vectors derived from AAV1 and AAV2[84]. They found that the mixing rate of helper plasmid DNA containing the capsid gene obtained from two different serotypes reflects the characteristic of the packaged AAV vector by the mosaic capsid. Concerning the infection mechanism of AAV, it can be explained why the mosaic AAV vector has two different characters derived from original serotypes. First, the AAV vectors are known to have different tropism for each serotype, which is considered to result from differences in their capsid proteins[85-87]. The AAV2.1 vector, composed of higher rate of capsid proteins of AAV2, is also thought to inherit this high neuronal directivity from the AAV2 vector. It is also known that the transgene delivery systems of AAV vectors differs among serotypes. At the first step of the infection, the capsid protein of virion attaches to the receptor in the plasma membrane and entries the cytoplasm via endocytosis (Fig. 3-1). It is known that the trafficking system via plasma membrane is different among the serotypes of AAV. Glycan receptors on plasma membrane are famous as the receptor for many viruses and different AAV serotypes interact with different glycan receptors. Heparan sulfate proteoglycans (HSPG) are one of the first receptor of AAV2, whereas AAV1 does not interact with it[88-92]. AAV1 interacts with the sialic acid (SIA) receptors for cell entry[92]. Even though the cell entry mechanism of AAV1 has not yet been known at that time, Rabinowitz et al. has suggested that the trafficking system of the mosaic AAV vector through the plasma membrane may be controlled by the AAV1 portion of the virion by a

route distinct from that used by AAV2[58]. Furthermore, as Rabinowitz et al. reported, a mosaic vector of AAV2 and AAV5 containing 75% of the AAV2 capsid proteins does not bind to HSPG[47]. This suggests that the AAV2.1-B vector, which is combined with 50% of AAV1 capsid and 50% of AAV2 capsid, might not bind to HSPG and only binds to SIA. This could explain why the AAV2.1-B vector showed the characteristics similar to the AAV1 vector (i.e., glial infectivity). Additionally, it has been shown that the mosaic vectors including 10% capsid protein of AAV5 successfully bind to mucin, which is known as the glycoprotein binding with SIA[47,92]. It is known that the AAV5 binds to SIA, as well as AAV1. Although the AAV2.1-A vector contains only 10% of the capsid protein of AAV1, there is a high possibility that the AAV2.1-A vector can bind to both receptors of AAV1 and AAV2. In addition, neurons are known as rich in HSPG. The reason why AAV2.1 vectors have high neuron-specificity could be hypothesized to be due to their high proportion of AAV2 capsids, which increase the possibility of binding to HSPG on neurons. However, it has been reported that the serotype-specific characteristics of certain cell types are expressed not in the cell entry mechanism, but in the gene expression process[93,94]. Therefore, we must exercise caution when discussing the mechanisms of AAV vector tropism based solely on differences in receptors on the plasma membrane.

In considering the reasons why the AAV2.1 vector has achieved higher transgene expression levels than the AAV2 vector, insights may be gained by examining the transporting mechanism of AAV particles. AAV particles internalized and transported by endosome are released from endosome to enter the nucleus. It is considered that phospholipase A2 (PLA2), which is present in capsid protein, might be involved in their escape from endosomes[95,96]. Previous studies have suggested that the efficiency of

endosomal escape and the efficiency of uncoating (release of viral DNA from the AAV capsid particle after endosomal escape) may differ among serotypes[47,97,98]. It is known that the AAV2 capsid has the problem to endosomal escape from endosome but the AAV1 capsid is easy to escape from endosome[47]. AAV2 shows to be a less efficient uncoating serotype, while AAV1 is more efficient uncoating serotypes[99]. It suggested that the AAV2.1 vector, which composed of capsid protein of AAV1 and AAV2, may achieve high expression efficiency due to the efficient uncoating from AAV1 capsid[97,98]. In conclusion, the AAV2.1 vector may achieve neuron-specificity and high transgene expression levels by combining the efficient infection of neuron provided by AAV2 capsid with the efficient nuclear gene transfer of AAV1 capsid.

3.3. Advantage of AAV2.1 vector in neurodegenerative diseases model of primates

For these decades, particular attention has been attracted to create various animal models of neurological diseases by using viral vectors. In a Parkinson's disease model, for example, overexpression of α-synuclein in the substantia nigra by the AAV vector causes degeneration and loss of dopamine neurons over time after vector injection, eventually resulting in severe motor deficits, such as those observed in Parkinson's disease at 12 weeks after injection[100]. Long-term behavioral data are essential for the observation of such neurodegenerative diseases. Even if a viral vector is used to induce neurodegeneration and behavioral changes, the viral vector itself may cause severe inflammation and cell death around the injection site. The side effects caused by the viral vector infection make it difficult to determine what in fact causes behavioral impairments. Especially in the animal models of neurodegenerative diseases that cause cell death, such as the Parkinson's disease model, it is necessary to clearly distinguish whether the protein introduced by the viral vector induces neurodegeneration or the infection of viral vector causes neurodegeneration through the inflammation. While the AAV vectors such as AAV2 with the property of high neuronal specificity are used to avoid immune response, the transgene expression levels may not be sufficient to induce some neurological disorders. Indeed, viral vectors exhibiting high transgene expression levels are often employed in the creation of animal models of neurodegenerative diseases. However, the effects of immune responses induced by non-specific infection of these viral vectors have rarely been examined. Viral vectors such as the AAV2.1 vector, which show stable and high transgene expression levels over a long period of time and exhibit neuron specificity, are likely to be useful in the creation of animal models of neurological diseases.

Viral vectors with high neuron specificity are useful not only in creation of disease models but also in therapeutic studies. In case of inhibition of seizure in epilepsy model through neural circuit manipulation, the AAV2.1 vector has already utilized. In the recent study[101], the epilepsy model was created by injection of bicuculine into the forelimb region of M1 in macaque monkeys, and AAV2.1 was used to express inhibitory DREADD receptors in the region where neural activity caused by seizures occurred. In the present study, histological assessment showed that DREADD-expressing region transduced by the AAV2.1 vector did not cause any undue tissue damage. As noted earlier, in studies of neurological disorder models, brain tissue damage caused by inflammatory response to foreign proteins expressed by viral vectors or to viral vectors themselves can hinder interpreting the results of neural circuit manipulation caused by viral vectors. This research suggested that the utility of low-inflammatory property of the AAV2.1 vector with excellence in neuron-specificity in the primate brain. Only the AAV2.1 vector carrying the inhibitory DREADD receptor was utilized in this study; however, numerous other studies have demonstrated that both inhibitory and excitatory DREADD receptors, individually expressed by the AAV2.1 vector, can be effectively applied in long-term experiments in various areas of the primate brain without causing inflammatory problems[102-105]. The AAV2.1 vector is becoming a powerful candidate for inducing/recovering neurodegenerative diseases models by excitatory/inhibitory chemogenetic neural circuit manipulation.

3.4 Conclusion and future perspectives

In the present study, it has been demonstrated that the AAV2.1 vector achieved both high efficiency of gene transduction and high neuron specificity in the primate brains. Moreover, applications of the AAV2.1 vector to chemogenetic manipulation and *in vivo* calcium imaging of neuronal activity have been introduced. Collectively, the AAV2.1 vector can be a versatile tool for diverse approaches in the primate brain, and the widespread and effective application of the AAV2.1-A vector not only could facilitate elucidating neural network mechanisms underlying various brain functions, but also might subserve the development valid primate models of neurological/psychiatric disorders.

The utility of the AAV2.1 vector is still expected to undergo further development. First, only limited combination patterns of the two serotypes (AAV2:AAV1 = 1:1 or 9:1) was attempted in this study. This is because preliminary *in vitro* experiments had already shown that the combination of a small percentage of AAV1 capsid with AAV2 significantly alters gene expression property. Optimal conditions for achieving both high gene expression efficiency and neuronal specificity in *in vivo* studies have not been examined. Particularly in animal experiments using primates, reduction in the number of animals used is strongly demanded, and it is difficult to conduct experiments to examine optimal conditions that require many sacrifices. However, experiments using brain organoids, which have been actively developed in recent years, might offer a potential solution to this problem. By optimization of the combination ratios of multiple serotypes in more brain-like *in vitro* systems like a brain organoid, and then only conducting final evaluations *in vivo*, even limited number of experimental animals may allow us to explore optimal conditions in the future. Especially in the comparison of viral vector properties

in primate brains, it is important to examine the immune response to viral vectors, but it is currently difficult to conduct such examinations *in vitro* systems. If primate brain organoids that can replicate the complex immune system close to *in vivo* conditions are developed, it could significantly change the environment of developing the viral vectors for primates. The creation of neurospheres using iPS cells from Japanese macaques has already been successful[106], and the development of more matured *in vitro* brain models that replicate the brain structure of primates is expected in the future.

Second, although the AAV2.1 vector developed in this study is a mosaic AAV vector composed of AAV1 and AAV2, the properties of mosaic vectors composed of combinations of other serotypes should also be investigated. In this study, AAV2 was selected as the only conventional serotype known to be highly specific to neurons, but there are many other serotypes with high expression efficiency besides AAV1. For example, AAV8 and AAV9 are serotypes with relatively high gene efficiency like AAV1, but each is known to be transported intracellularly via different pathways with AAV1 and AAV2[107-109]. The hypothesis that the capsid proteins of different AAV serotypes characterize not only their directivity but also their expression efficiency needs to be explored. Investigation of various combinations of capsid proteins may lead to mosaic AAV vectors with both higher gene expression efficiency and neuronal specificity, as well as provide useful insights into the gene transport mechanisms of each AAV serotype, which still remain unclear.

Although there are still issues to be considered regarding the optimization of mosaic AAV vectors in terms of capsid ratio and serotype combination, the development goal of "coexistence of neuronal specificity (i.e., low inflammation) and gene expression efficiency" set in this study provides a valuable inspiration for the future research for new

viral vectors. As well as mosaic capsid methods, various other approaches have been used to develop new AAV vectors. If new AAV vectors that focus on these two characteristics are developed, other novel AAV vectors may be promising candidates for primate neural circuit manipulation in addition to the AAV2.1 vector. The development of AAV vectors that achieve high gene transduction efficiency while avoiding the response of sensitive immune system of primates has been limited. This has led to uncertainties in long-term neural circuit manipulation experiments in primates, including the occurrence of inflammation and insufficient transgene expression levels. I believe that the AAV2.1 vector developed in this study will not only facilitate reliable neural circuit manipulation experiments in primates but also contribute to the discovery of new functions of neural circuits.

Acknowledgements

References

1. Human Brain Project. "Impressive research results - external review panel evaluates final results of Human Brain Project." https://www.humanbrainproject.eu/en/follow-hbp/news/2023/11/28/impressive-research-results-external-review-panel-evaluates-final-results-of-human-brain-project/ (2023).

2. Boyden, E.S., Zhang, F., Bamberg, E., Nagel, G. & Deisseroth, K. Millisecond-timescale, genetically targeted optical control of neural activity. *Nat. Neurosci.* **8**,1263-1268 (2005).

3. Deisseroth, K. Optogenetics. *Nat. Methods.* **8**, 26-29 (2011).

4. Deisseroth, K. Optogenetics: 10 years of microbial opsins in neuroscience. *Nat. Neurosci.* **18**, 1213-1225 (2015).

5. Strader, C. D., Gaffney, T., Sugg, E. E., Candelore, M.R., Keys, R., Patchett, A. A. & Dixon, R. A. Allele-specific activation of genetically engineered receptors. *J. Biol. Chem.* **266**, 5-8 (1991).

6. Sternson, S. M. & Roth, B. L. Chemogenetic tools to interrogate brain functions. *Annu. Rev. Neurosci.* **37**, 387-407 (2014).

7. Tremblay, S. *et al*. An open resource for non-human primate optogenetics. *Neuron* **108**, 1075-1090 (2020).

8. Roth, B. L. Primer DREADDs for neuroscientists. *Neuron* **89**, 683–694 (2016).

9. Armbruster, B. N., Li, X., Pausch, M. H., Herlitze, S. & Roth, B. L. Evolving the lock to fit the key to create a family of G protein-coupled receptors potently activated by an inert ligand. *Proc. Natl. Acad. Sci. USA* **104**, 5163–5168 (2007).

10. Oyama, K., *et al*. Chemogenetic dissection of the primate prefronto-subcortical pathways for working memory and decision-making. *Sci. Adv.* **7**, eabg4246 (2021).

11. Oguchi, M. *et al.* Chemogenetic inactivation reveals the inhibitory control function of the prefronto-striatal pathway in the macaque brain. *Commun. Biol.* **4**, 1088 (2021).

12. Guillamón-Vivancos, T., Vandael, D., Torres, D., López-Bendito, G. & Martini, F. J. Mesoscale calcium imaging in vivo: evolution and contribution to developmental neuroscience. *Front. Neurosci.* **17**, 1210199 (2023).

13. Watakabe, A. *et al*. Comparative analyses of adeno-associated viral vector serotypes 1, 2, 5, 8 and 9 in marmoset, mouse and macaque cerebral cortex. *Neurosci. Res.* **93**, 144–157 (2015).

14. Tanabe, S. *et al*. A note on retrograde gene transfer efficiency and inflammatory response of lentiviral vectors pseudotyped with FuG-E vs. FuG-B2 glycoproteins. *Sci. Rep.* **9**, 1–12 (2019).

15. Xu, X., *et al.* Viral vectors for neural circuit mapping and recent advances in trans-synaptic anterograde tracers. *Neuron* **107**, 1029-1047 (2020).

16. Naldini, L. *et al*. In vivo gene delivery and stable transduction of nondividing cells by a lentiviral vector. *Science* **272**, 263-267 (1996).

17. Naldini, L., Blömer, U., Gage, F. H., Trono, D. & Verma, I. M. Efficient transfer, integration, and sustained long-term expression of the transgene in adult rat brains injected with a lentiviral vector. *Proc. Natl. Acad. Sci. USA* **93**, 11382–11388 (1996).

18. Kriesel, F., Stegmann, L., Ciesek, S., Kaderali, L. & Baldauf, H.M. Efficient inactivation of pseudotyped HIV-based lentiviral vectors and infectious HIV. J Virol Methods. **276**, 113768 (2020).

19. Maes, M. E., Colombo, G., Schulz, R. & Siegert, S. Targeting microglia with lentivirus and AAV: Recent advances and remaining challenges. *Neurosci. Lett.* **707**, 134310 (2019).

20. Dong, B., Nakai, H. & Xiao, W. Characterization of genome integrity for oversized recombinant AAV vector. *Mol. Ther.* **18**, 87-92 (2010).

21. Wu, Z., Yang, H. & Colosi, P. Effect of genome size on AAV vector packaging. *Mol. Ther.* **18**, 80-86 (2010).

22. Diester, I. *et al*. An optogenetic toolbox designed for primates. *Nat. Neurosci.* **14**, 387-397 (2011).

23. Cavanaugh, J. *et al*. Optogenetic inactivation modifies monkey visuomotor behavior. *Neuron* **76**, 901–907 (2012).

24. Gerits, A. et al. Optogenetically induced behavioral and functional network changes in primates. *Curr. Biol.* **22**, 1722–1726 (2012).

25. Jazayeri, M., Lindbloom-brown, Z. & Horwitz, G. D. Saccadic eye movements evoked by optogenetic activation of primate V1. *Nat. Neurosci.* **15**, 11–14 (2012).

26. Ohayon, S., Grimaldi, P., Schweers, N. & Tsao, D. Y. Saccade modulation by optical and electrical stimulation in the macaque frontal eye field. *J. Neurosci.* **33**, 16684–16697 (2013).

27. Dai, J., Brooks, D. I. & Sheinberg, D. L. Report optogenetic and electrical microstimulation systematically bias visuospatial choice in primates. *Curr. Biol.* **24**, 63-69 (2014).

28. Afraz, A., Boyden, E. S., & Dicarlo, J. J. Optogenetic and pharmacological suppression of spatial clusters of face neurons reveal their causal role in face gender discrimination. *Proc. Natl. Acad. Sci. USA* **112**, 6730-6735 (2015).

29. Inoue, K., Takada, M. & Matsumoto, M. Neuronal and behavioural modulations by pathway-selective optogenetic stimulation of the primate oculomotor system. *Nat. Commun.* **6**, 1–7 (2015).

30. Stauffer, W. R. *et al*. Dopamine neuron-specific optogenetic stimulation in rhesus macaques. *Cell* **166**, 1564–1568 (2016).

31. Acker, L., Pino, E. N., Boyden, E. S., & Desimone, R. FEF inactivation with improved optogenetic methods. *Proc. Natl. Acad. Sci. USA* **113**, 7297–7306 (2016).

32. Galvan, X. A., Hu, X., Smith, Y., & Wichmann, T. (2016). Effects of optogenetic activation of corticothalamic terminals in the motor thalamus of awake monkeys. *J. Neurosci.* **36**, 3519–3530 (2016).

33. Nagai, Y. *et al*. PET imaging-guided chemogenetic silencing reveals a critical role of primate rostromedial caudate in reward evaluation. *Nat. Commun.* **7**, 1–8 (2016).

34. El-shamayleh, Y., Kojima, Y., Soetedjo, R. & Horwitz, G. D. Selective optogenetic control of purkinje cells in monkey cerebellum. Neuron 95, 51–62 (2017).

35. Tamura, K. *et al*. Conversion of object identity to object-general semantic value in the primate temporal cortex. *Science* **357**, 687–692 (2017).

36. O'Shea, D. J. *et al*. The need for calcium imaging in nonhuman primates: New motor neuroscience and brain-machine interfaces. *Exp. Neurol.* **287**, 437-451 (2017).

37. Ciesielska, A. *et al*. Cerebral infusion of AAV9 vector-encoding non-self proteins can elicit cell-mediated immune responses. *Mol. Ther.* **21**, 158–166 (2013).

38. Shirley, J. L., Jong, Y. P. de, Terhorst, C. & Herzog, R. W. Immune responses to viral gene therapy vectors. *Mol. Ther.* **28**, 709–722 (2020).

39. Verdera, H. C., Kuranda, K. & Mingozzi, F. AAV vector immunogenicity in humans : a long journey to successful gene transfer. *Mol. Ther.* **28**, 723–746 (2020).

40. Eldik, L. J. V., Thompson, W. L., Ranaivo, H. R., Behanna, H. A. & Watterson, D. M. Glia proinflammatory cytokine upregulation as a therapeutic target for

neurodegenerative diseases: function-based and target-based discovery approaches. *Int. Rev. Neurobiol.* **82**, 277-296 (2007).

41. Kotterman, M. A. &Schaffer, D. V. Engineering adeno-associated viruses for clinical gene therapy. *Nat. Rev. Genet.* **15**, 445-451 (2014).

42. Lin, R. *et al.* Directed evolution of adeno-associated virus for efficient gene delivery to microglia. *Nat. Methods.* **19**, 976-985 (2022).

43. Tervo, D. G. R. *et al.* A designer AAV variant permits efficient retrograde access to projection neurons. *Neuron* **92**, 372-382 (2016).

44. Deverman, B. E., *et al.* Cre-dependent selection yields AAV variants for widespread gene transfer to the adult brain. *Nat. Biotechnol.* **34**, 204-209 (2016).

45. Chan, K. Y. et al. Engineered AAVs for efficient noninvasive gene delivery to the central and peripheral nervous systems. *Nat. Neurosci.* **20**, 1172-1179 (2017).

46. Hauck, B., Chen, L. & Xiao, W. Generation and characterization of chimeric recombinant AAV vectors. *Mol. Ther.* **7**, 419–25 (2003).

47. Rabinowitz, J. E. *et al.* Cross-dressing the virion: the transcapsidation of adeno-associated virus serotypes functionally defines subgroups. *J. Virol.* **78**, 4421–32 (2004).

48. Adamantidis, A. R., Zhang, F., Aravanis, A. M., Deisseroth, K. & Lecea, L. de. Neural substrates of awakening probed with optogenetic control of hypocretin neurons. *Nature* **450**, 420-424 (2007).

49. Gradinaru, V., Mogri, M. Z., Thompson, K. R., Henderson, J. M. & Deisseroth, K. Optical deconstruction of parkinsonian neural circuitry. *Science* **324**, 354–359 (2009).

50. Zhang, F. *et al.* Optogenetic interrogation of neural circuits: technology for probing mammalian brain structures. *Nat. Protoc.* **5**, 439–456 (2010).

51. Galvan, A. *et al*. Nonhuman primate optogenetics: recent advances and future directions. *J. Neurosci.* **37**, 10894–10903 (2017).

52. Atasoy, D. & Sternson, S. M. Chemogenetic tools for causal cellular and neuronal biology. *Physiol. Rev.* **98**, 391-418 (2018).

53. Alexander, G. M. *et al*. Remote control of neuronal activity in transgenic mice expressing evolved G protein-coupled receptors. *Neuron* **63**, 27-39 (2009).

54. Tye, K. M. & Deisseroth, K. Optogenetic investigation of neural circuits underlying brain disease in animal models. *Nat. Rev. Neurosci.* **13**, 251-266 (2012).

55. Zincarelli, C., Soltys, S., Rengo, G. & Rabinowitz, J. E. Analysis of AAV serotypes 1-9 mediated gene expression and tropism in mice after systemic injection. *Mol. Ther.* **16**, 1073–1080 (2008).

56. Srivastava, A. In vivo tissue-tropism of adeno-associated viral vectors. *Curr. Opin. Virol.* **21**, 75–80 (2016).

57. Klein, C. *et al*. Cell-targeted optogenetics and electrical microstimulation reveal the primate koniocellular projection to supra-granular visual cortex. *Neuron* **90**, 143–151 (2016).

58. Hadaczek, P. *et al*. Transduction of nonhuman primate brain with Adeno-associated virus serotype 1: vector trafficking and immune response. *Hum. Gene. Ther.* **20**, 225–237 (2009).

59. Markakis, E. A. *et al*. Comparative transduction efficiency of AAV vector serotypes 1 – 6 in the substantia nigra and striatum of the primate brain. *Mol. Ther.* **18**, 588–593 (2010).

60. Samaranch, L. *et al*. AAV9-mediated expression of a non-self protein in nonhuman primate central nervous system triggers widespread neuroinflammation driven by antigen-presenting cell transduction. *Mol. Ther.* **22**, 329–337 (2014).

61. Fiandaca, M., Forsayeth, J. & Bankiewicz, K. Current status of gene therapy trials for Parkinson's disease. *Exp. Neurol.* **209**, 51–57 (2008).

62. Mueller, C. & Flotte, T. R. Clinical gene therapy using recombinant adeno-associated virus vectors. *Gene. Ther.* **15**, 858-863 (2008).

63. Russell, S. et al. Efficacy and safety of voretigene neparvovec (AAV2-hRPE65v2) in patients with RPE65 -mediated inherited retinal dystrophy: a randomised, controlled, open-label, phase 3 trial. *Lancet* **390**, 849–860 (2017).

64. Domenger, C. & Grimm, D. Next-generation AAV vectors — do not judge a virus (only) by its cover. *Hum. Mol. Genet.* **28**, R3–R14 (2019).

65. Choi, V. W., McCarty, D. M. & Samulski, R. J. AAV hybrid serotypes: improved vectors for gene delivery. *Curr. Gene. Ther.* **5**, 299-310 (2005).

66. Nagai, Y. *et al*. Deschloroclozapine, a potent and selective chemogenetic actuator enables rapid neuronal and behavioral modulations in mice and monkeys. *Nat. Neurosci.* **23**, 1157-1167 (2020).

67. Ichise, M. *et al*. Noninvasive quantification of dopamine D2 receptors with iodine-123-IBF SPECT. *J. Nucl. Med.* **37**, 513-520 (1996).

68. Fang, Y. *et al*. An orientation map for disparity-defined edges in area V4. *Cereb. Cortex* 29, 666-679 (2018).

69. Li, M., Liu, F., Jiang, H., Lee, T. S. & Tang, S. Long-term two-photon imaging in awake macaque monkey. *Neuron* **93**, 1049-1057 (2017).

70. Ikezoe, K., Mori, Y., Kitamura, K., Tamura, H. & Fujita, I. Relationship between the local structure of orientation map and the strength of orientation tuning of neurons in monkey V1: a 2-photon calcium imaging study. *J. Neurosci.* **33**, 16818-16827 (2013).

71. Ikezoe, K., Amano, M., Nishimoto, S. & Fujita, I. Mapping stimulus feature selectivity in macaque V1 by two-photon Ca2+ imaging: encoding-model analysis of fluorescence responses to natural movies. *NeuroImage* **180** (Pt A), 312-323 (2018).

72. Schindelin, J. *et al*. Fiji: an open-source platform for biological-image analysis. *Nat. Methods* **9**, 676-682 (2012).

73. Dayton, R. D. *et al*. Frontotemporal lobar degeneration-related proteins induce only subtle memory-related deficits when bilaterally overexpressed in the dorsal hippocampus. *Exp. Neurol*. **233**, 807-814 (2012).

74. Kubota, S. *et al*. Optogenetic recruitment of spinal reflex pathways from large-diameter primary afferents in non-transgenic rats transduced with AAV9/Channelrhodopsin 2. *J. Physiol*. **597**, 5025-5040 (2019).

75. Papp, M. *et al*. AMPA receptors mediate the pro-cognitive effects of electrical and optogenetic stimulation of the medial prefrontal. *J. Psychopharmacol*. **34**, 1418-1430 (2020).

76. Phelps, M. E. *et al*. Tomographic measurement of local cerebral glucose metabolic rate in humans with validation of method. *Ann. Neurol.* **6**, 371–388 (1978).

77. Poremba, A. *et al*. Species-specific calls evoke asymmetric activity in the monkey's temporal poles. *Nature* **427**, 448–451 (2004).

78. Michaelides, M. *et al*. Whole-brain circuit dissection in free-moving animals reveals cell-specific mesocorticolimbic networks. *J. Clin Invest.* **123**, 5342–5350 (2013).

79. Zhou, Y., Aran, J., Gottesman, M. M. & Pastan, I. Co-expression of human adenosine deaminase and multidrug resistance using a bicistronic retroviral vector. *Hum. Gene. Ther.* **9**, 287-293 (1998).

80. Mizuguchi, H., Xu, Z., Ishii-Watabe, A., Uchida, E. & Hayakawa, T. IRES-dependent second gene expression is significantly lower than cap-dependent first gene expression in a bicistronic vector. *Mol. Ther.* **1**, 376-382 (2000).

81. Fuler, S., Paterna, J. C., Weibel, M. & Büeler, H. Recombinant AAV vectors containing the foot and mouth disease virus 2A sequence confer efficient bicistronic gene expression in cultured cells and rat substantia nigra neurons. *Gene. Ther.* **8**, 864-873 (2001).

82. Earley, L. F., *et al.* Adeno-associated virus serotype-specific inverted terminal repeat sequence role in vector transgene expression. *Hum. Gene. Ther.* **31**, 151-162 (2020).

83. Gray, S. J. *et al.* Preclinical differences of intravascular AAV9 delivery to neurons and glia: a comparative study of adult mice and nonhuman primates. *Mol. Ther.* **19**, 1058–1069 (2011).

84. Rabinowitz, J. E., Rolling, F., Li, C., Conrath, H., Xiao, W., Xiao, X. & Samulski, R. J. Cross-packaging of a single adeno-associated virus (AAV) type 2 vector genome into multiple AAV serotypes enables transduction with broad specificity. *J. Virol.* **76**, 791-801 (2002).

85. Mulcrone, P. L., Lam, A. K., Frabutt, D., Zhang, J., Chrzanowski, M., Herzog, R.W. & Xiao, W. Chemical modification of AAV9 capsid with N-ethyl maleimide alters vector tissue tropism. Sci. Rep., 11, (2021).

86. Xie, Y. & Butler, M. N-glycomic profiling of capsid proteins from adeno-associated virus serotypes. *Glycobiology* **9**, cwad074 (2023).

87. Keng, C. T., *et al*. Multiplex viral tropism assay in complex cell populations with single-cell resolution. *Gene. Ther.* **29**, 555-565 (2022).

88. Summerford, C. & Samulski, R. J. Membrane-associated heparan sulfate proteoglycan is a receptor for adeno-associated virus type 2 virions. *J. Virol.* **72**, 1438-1445 (1998).

89. Qing, K., Mah, C., Hansen, J., Zhou, S., Dwarki, V. & Srivastava, A. Human fibroblast growth factor receptor 1 is a co-receptor for infection by adeno-associated virus 2. *Nat. Med.* **5**, 71-77 (1999).

90. Summerford, C., Bartlett, J.S. & Samulski, R. J. AlphaVbeta5 integrin: a co-receptor for adeno-associated virus type 2 infection. *Nat. Med.* **5**, 78-82 (1999).

91. Schmidt, M., Govindasamy, L., Afione, S., Kaludov, N., Agbandje-McKenna, M. & Chiorini, J. A. Molecular characterization of the heparin-dependent transduction domain on the capsid of a novel adeno-associated virus isolate, AAV(VR-942). *J. Virol.* **82**, 8911–8916 (2008).

92. Huang, L. Y., *et al*. Characterization of the adeno-associated virus 1 and 6 sialic acid binding site. *J. Virol.* **90**, 5219-5230 (2016).

93. Hansen, J., Qing, K., Kwon, H. J., Mah, C. & Srivastava, A. Impaired intracellular trafficking of adeno-associated virus type 2 vectors limits efficient transduction of murine fibroblasts. *J. Viol.* **74**, 992-996 (2000).

94. Hansen, J., Qing, K. & Srivastava, A. Adeno-associated virus type 2-mediated gene transfer: altered endocytic processing enhances transduction efficiency in murine fibroblasts. *J. Viol.* **75**, 4080-4090 (2001).

95. Girod, A., et al. The VP1 capsid protein of adeno-associated virus type 2 is carrying a phospholipase A2 domain required for virus infectivity. *J. Gen. Virol.* **83**, 973-978 (2002).

96. Hermonat, P. L., Labow, M. A., Wright, R., Berns, K. I. & Muzyczka, N. Genetics of adeno-associated virus: isolation and preliminary characterization of adeno-associated virus type 2 mutants. *J. Viol.* **51**, 329-339 (1984).

97. Wang, J., Faust, S. M. & Rabinowitz, J. E. The next step in gene delivery: molecular engineering of adeno-associated virus serotypes. *J. Mol. Cell. Cardiol.* **50**, 793-802 (2011).

98. Thomas, C. E., Storm, T. A., Huand, Z. & Kay, M. A. Rapid uncoating of vector genomes is the key to efficient liver transduction with pseudotyped adeno-associated virus vectors. *J. Virol.* **78**, 3110-3122 (2004).

99. Keiser, N., Yan, Z., Zhang, Y., Lei-Butters, D. C. M. & Engelhardt, J. F. Unique characteristics of AAV1, 2, and 5 viral entry, intracellular trafficking, and nuclear import define transduction efficiency in HeLa cells. *Hum. Gene. Ther.* **22**, 1433-1444 (2011).

100. Song, L. K., *et al*. Targeted overexpression of α-Synuclein by rAAV2/1 vectors induces progressive nigrostriatal degeneration and increases vulnerability to MPTP in mouse. *PLoS One*. **10**, e0131281 (2015).

101. Miyakawa, N., *et al*. Chemogenetic attenuation of cortical seizures in nonhuman primates. *Nat. Commun.* **14**, 971 (2023).

102. Hori, Y., *et al*. Single caudate neurons encode temporally discounted value for formulating motivation for action. *eLife* **10**, e61248. (2021).

103.   Mimura, K., *et al*. Chemogenetic activation of nigrostriatal dopamine neurons in freely moving common marmosets. *iScience* **24**, 103066 (2021).

104.   Hirabayashi, T., *et al*. Chemogenetic sensory fMRI reveals behaviorally relevant bidirectional changes in primate somatosensory network. *Neuron* **109**, 3312-3322.e5 (2021).

105.   Hori, Y., et al. Multimodal imaging for validation and optimization of ion channel-based chemogenetics in nonhuman primates. *J. Neurosci.* **43**, 6619-6627 (2023).

106.   Nakai, R., *et al*. Early neurogenic properties of iPSC-derived neurosphere formation in Japanese macaque monkeys. *Diffeerntiation* **128**, 33-42 (2022).

107.   Mulcrone, P. L., Lam, A. K., Frabutt, D., Zhang, J., Chrzanowski, M., Herzog, R. W. & Xiao, W. Chemical modification of AAV9 capsid with N-ethyl maleimide alters vector tissue tropism. *Sci. Rep*. **13**, 8436 (2023).

108.   Bantel-Schaal, U., Hub, B. & Kartenbeck, J. Endocytosis of adeno-associated virus type 5 leads to accumulation of virus particles in the Golgi compartment. *J. Virol.* **76**, 2340-2349 (2002).

109.   Akache, B., Grimm, D., Pandey, K., Yant, S. R., Xu, H. & Kay, M. A. The 37/67-kilodalton laminin receptor is a receptor for adeno-associated virus serotypes 8, 2, 3, and 9. *J. Virol*. **80**, 9831-9836 (2006).

Table

Table 1. Summary of recombinant AAV vectors for macaque monkeys

| Animal ID | Serotype | % Capsid | | Promoter | Gene | Stock titer (gc/ml) | Injection titer (gc/ml) |
		AAV1	AAV2				
Monkey A	AAV2	0	100	CMV	mKO1	5.0×10^{13}	1.5×10^{13}
Monkey B				Syn	mKO1	8.0×10^{13}	6.0×10^{13}
	AAV2.1-A	10	90	CMV	mKO1 (i)	2.2×10^{14}	1.5×10^{13}
				Syn	mKO1 (ii)	2.8×10^{14}	6.0×10^{13}
	AAV2.1-B	50	50	CMV	mKO1	9.3×10^{14}	1.5×10^{13}
				Syn	mKO1	1.0×10^{15}	6.0×10^{13}
	AAV1	100	0	CMV	mKO1	7.7×10^{14}	1.5×10^{13}
				Syn	mKO1 (iii)	8.4×10^{14}	6.0×10^{13}
Monkey C	AAV2.1-A	10	90	CMV	mKO1	s.a. (i)	1.5×10^{13}
Monkey D				Syn	mKO1	s.a. (ii)	6.0×10^{13}
	AAV1	100	0	CMV	mKO1	8.5×10^{14}	1.5×10^{13}
				Syn	mKO1	s.a. (iii)	6.0×10^{13}
	AAV5	-	-	CMV	mKO1	5.0×10^{14}	1.5×10^{13}
				Syn	mKO1	9.5×10^{14}	6.0×10^{13}
	AAV9	-	-	CMV	mKO1	1.4×10^{15}	1.5×10^{13}
				Syn	mKO1	1.3×10^{15}	6.0×10^{13}
Monkey E	AAV2	0	100	Syn	hM3Dq-IRES-AcGFP	1.8×10^{13}	1.0×10^{13}
	AAV2	0	100	CMV	hM3Dq-IRES-AcGFP	1.0×10^{13}	1.0×10^{13}
	AAV2.1-A	10	90	Syn	hM3Dq-IRES-AcGFP	5.0×10^{13}	1.0×10^{13} 5.0×10^{13}
Monkey F	AAV2	0	100	Syn	hM3Dq	1.0×10^{14}	2.0×10^{13}
	AAV2	0	100	Syn	hM3Dq-IRES-AcGFP	2.0×10^{13}	2.0×10^{13}
	AAV2.1-A	10	90	Syn	hM3Dq-IRES-AcGFP	4.0×10^{13}	2.0×10^{13}
	AAV1	100	0	Syn	hM3Dq-IRES-AcGFP	8.9×10^{13}	2.0×10^{13}
Monkey G	AAV2.1-A	10	90	CaMKIIα	GCaMP6s (iv)	1.2×10^{14}	1.0×10^{14} 2.0×10^{13}
				Syn		1.2×10^{14}	1.0×10^{14} 2.0×10^{13}
Monkey H	AAV2.1-A	10	90	CaMKIIα	GCaMP6s	s.a. (iv)	4.0×10^{13}

s.a., same as.

Figures
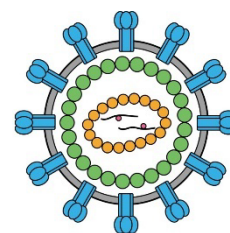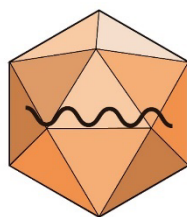
Virus	Adeno-associated Virus (AAV)	Lentivirus
Family	Parvoviridae	Retroviridae
Enveloped	no	yes
Genome type	(+) ssDNA	(+) ssRNA
Vector capacity	~4.8 kb	~8 kb
Biosafety level	BSL1	BSL2
Advantages	Non-pathogenic	Stable and persistent transgene expression
Disadvantages	Low capacity	Potential for oncogenesis

Fig.1-1 Comparison of the characteristics of adeno-associated virus and lentivirus, commonly employed for gene delivery in neuroscience research

Adeno-associated virus (AAV) and lentivirus, known as the commonly employed viral vector, is compared in terms of the characteristics of virus, capacity of transgene delivery, classification of biosafety level (BSL), advantages and disadvantages for gene delivery. This figure and table are adapted and rendered based on relevant information in Xu et al. (2020). The virion images are newly illustrated. (+) ssDNA, positive-sense single-stranded DNA. (+) ssRNA, positive-sense single-stranded RNA. BSL, biosafety level.
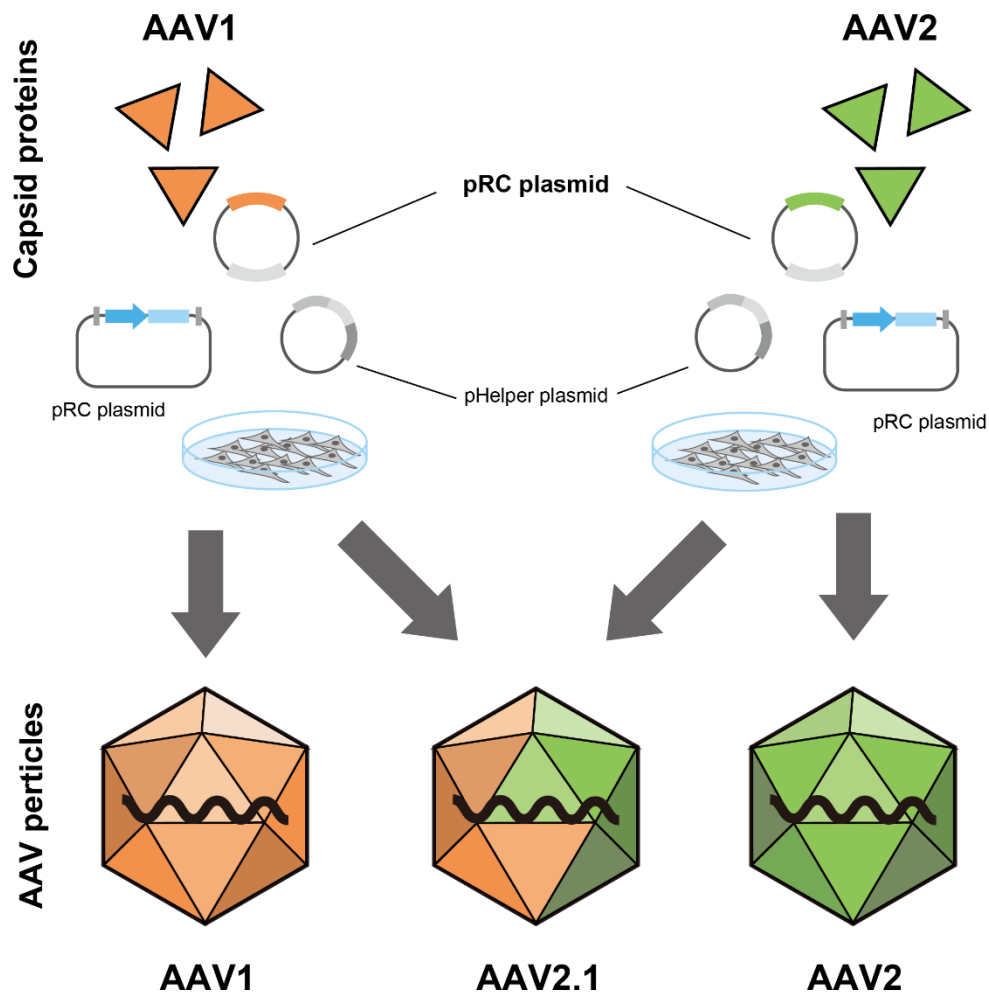
Fig.1-2 Production of mosaic AAV vector

The simplified process of mosaic AAV vector production is illustrated. Through the basic AAV vector production process, plasmids encoding capsid proteins (pRC plasmid) are introduced into the cultured cells to duplicate the capsid proteins and viral vector genes. To create mosaic AAV vector, two types of plasmids originated from two different serotypes (i.e., AAV1 and AAV2) was introduced into the cells. Two different plasmids encoding different capsid sequences from AAV1 and AAV2 are produced both capsid proteins in the single cell, and the viral genomes are packaged with mosaic capsid consist of two different capsid proteins. As described in the results of Chapter 2, we have

developed two types of mosaic AAV vectors by changing the mixture rate of these plasmids.
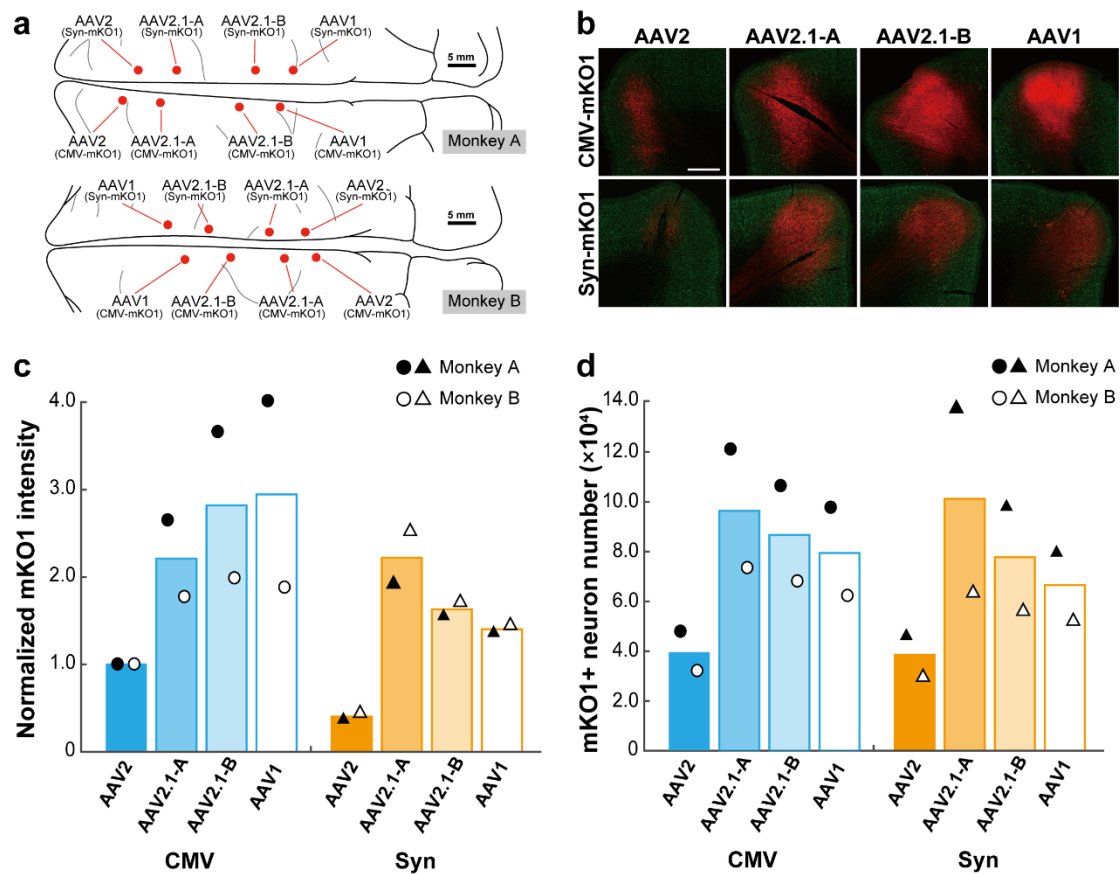
Fig. 2-1. Intensity of mKO1 native-fluorescence and number of mKO1-positive neurons at sites of monkey cortical injections of AAV2, AAV2.1-A, AAV2.1-B, and AAV1 vectors. (**a**) Schematic diagrams showing the injection loci of eight distinct types of recombinant AAV vectors carrying the mKO1 gene in the medial wall of the frontal lobe in Monkey A (upper) and Monkey B (lower). Scale bars, 5 mm. (**b**) mKO1 native-fluorescence (red) and NeuN immunofluorescence (green) at each vector injection site. Representative images from Monkey A. Similar observations were made for monkey B. Scale bar, 1 mm. (**c**) Comparison of mKO1 native-fluorescence intensity within a 2-mm-diameter circular observation window. Data are expressed as the averaged value obtained in Monkeys A (filled symbols) and B (open symbols), relative to the mean for the AAV2-CMV vector

defined as 1.0. (**d**) Comparison of mKO1-positive neuron number obtained from stereological cell counts. The cell counts were done over the whole transgene-expressing region in each section. n=2 biologically independent animals. See the Methods for the details of fluorescence intensity and cell-count analyses. Source data are provided as a Source data file.
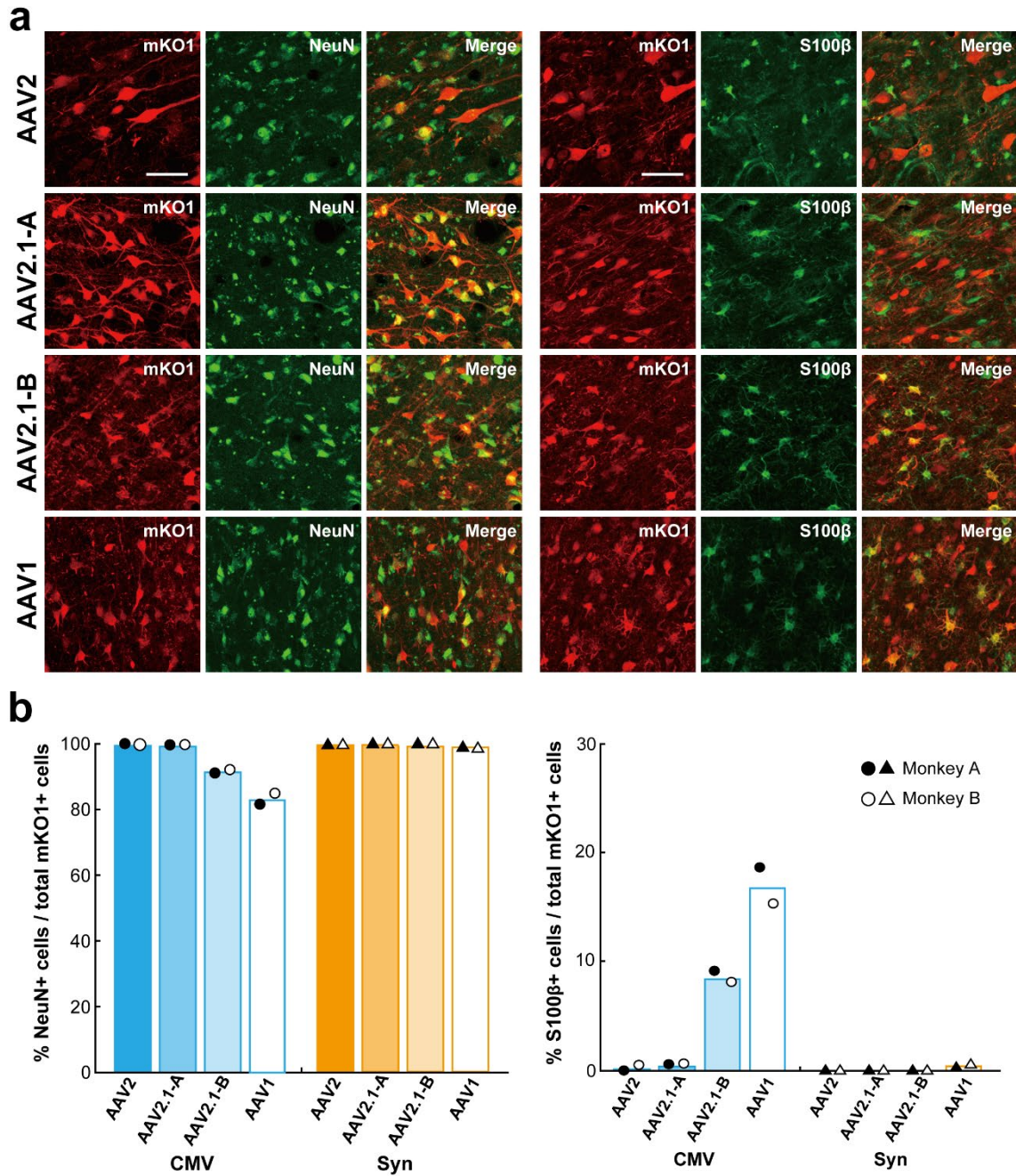
Fig. 2-2. Transgene expression in neurons and glial cells at injection sites of AAV2, AAV2.1-A, AAV2.1-B, and AAV1 vectors.

(**a**) Double fluorescence histochemistry for mKO1 native-fluorescence (red) and immunofluorescence for NeuN (green; left) or S100β (green; right) at the injection sites of AAV vectors inserted with CMV promoter. Shown are representative images obtained

in Monkey A. In each case, double-labeled cells are denoted in yellow (Merge). Representative images from Monkey A. Similar observations were made for monkey B. Scale bars, 50 μm. (**b**) Ratios of cells double-labeled for NeuN (left) or S100β (right) to the total mKO1-positive cells at each vector injection site. Each ratio was determined as the mean of data obtained in three sections examined, including the section through the center of the injection site. n=2 biologically independent animals. Source data are provided as a Source data file.
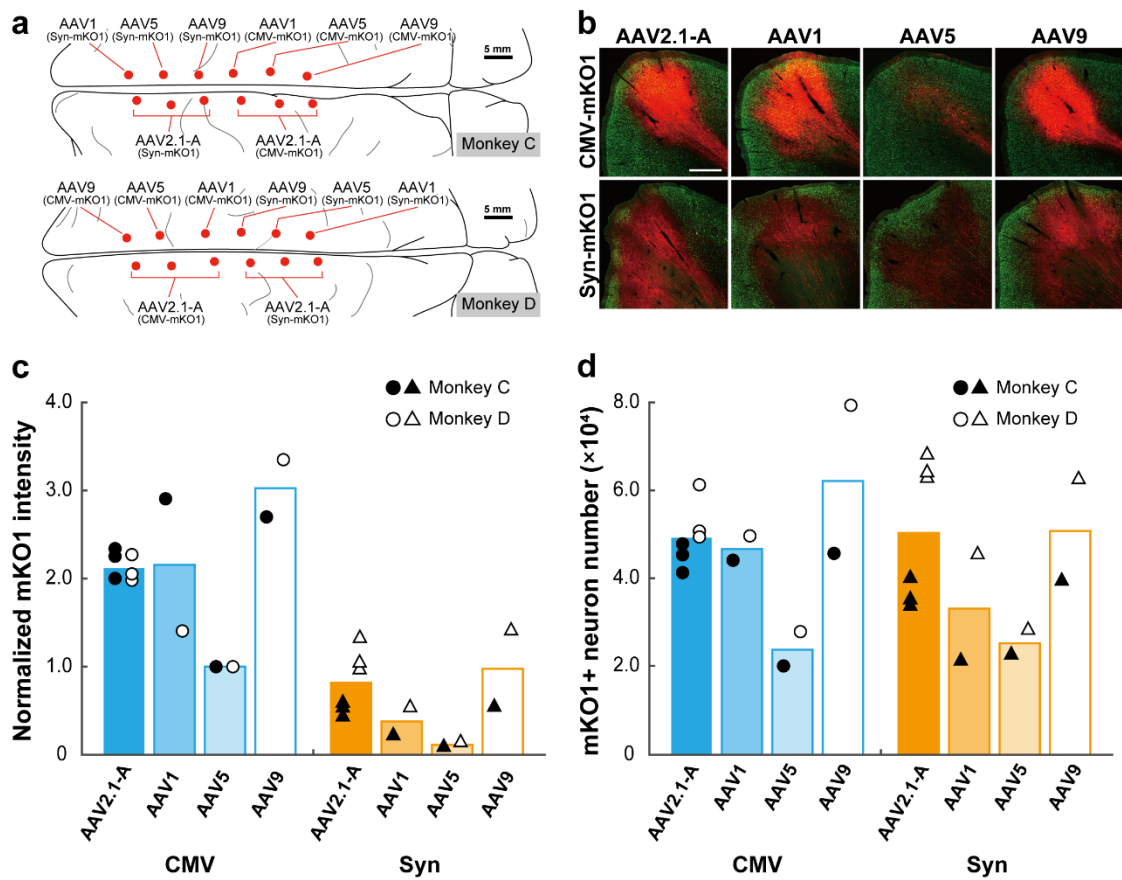
Fig. 2-3. Intensity of mKO1 native-fluorescence and number of mKO1-positive neurons at sites of monkey cortical injections of AAV2.1-A, AAV1, AAV5, and AAV9 vectors.

(**a**) Schematic diagrams showing the injection loci of eight distinct types of recombinant AAV vectors carrying the mKO1 gene in the medial wall of the frontal lobe in Monkey C (upper) and Monkey D (lower). The sites of cortical injections of the AAV2.1-A vector were placed symmetrically to those of the other vectors in the opposite hemisphere. Scale bars, 5 mm. (**b**) mKO1 native-fluorescence (red) and NeuN immunofluorescence (green) at each vector injection site. Representative images from Monkey C. Similar observations were made for monkey D. Scale bar, 1 mm. (**c**) Comparison of mKO1 native-fluorescence intensity within a 2-mm-diameter circular observation window. Data are expressed as the averaged value obtained in Monkeys C (filled symbols) and D (open symbols), relative to the mean for the AAV5-CMV vector defined as 1.0. (**d**) Comparison of mKO1-positive

neuron number obtained from stereological cell counts. The cell counts were done over the whole transgene-expressing region in each section. See the Methods for the details of fluorescence intensity and cell-count analyses. n=2 biologically independent animals. Source data are provided as a Source data file.
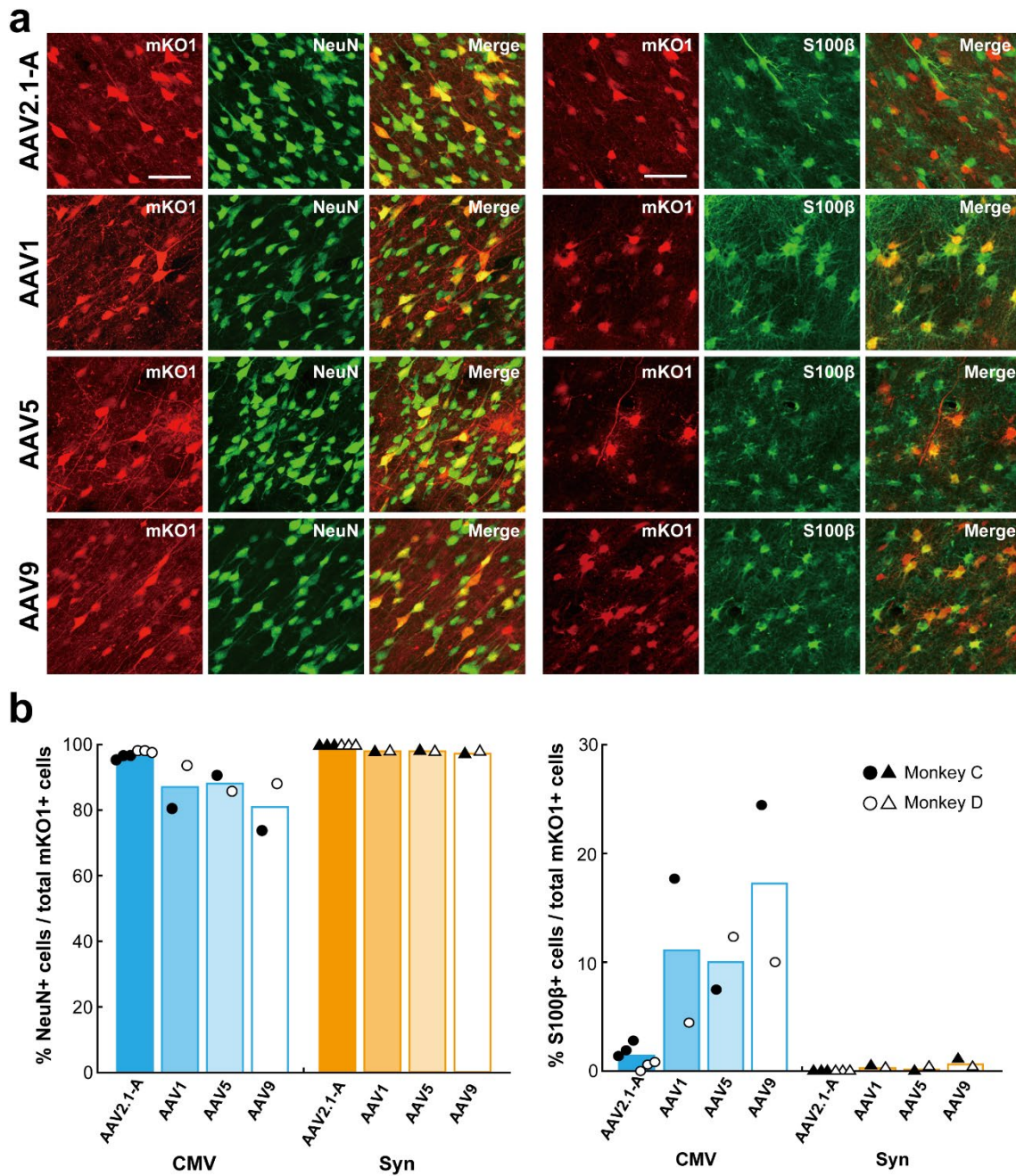
Fig. 2-4. Transgene expression in neurons and glial cells at injection sites of AAV2.1-A, AAV1, AAV5, and AAV9 vectors.

(**a**) Double fluorescence histochemistry for mKO1 native-fluorescence (red) and immunofluorescence for NeuN (green; left) or S100β (green; right) at the injection sites

78

of AAV vectors inserted with CMV promoter. Shown are representative images obtained in Monkey C. In each case, double-labeled cells are denoted in yellow (Merge). Representative images from Monkey C. Similar observations were made for monkey D. Scale bars, 50 μm. (**b**) Ratios of cells double-labeled for NeuN (left) or S100β (right) to the total mKO1-positive cells at each vector injection site. Each ratio was determined as the mean of data obtained in three sections examined, including the section through the center of the injection site. n=2 biologically independent animals, and n=6 independent injections for the AAV2.1-A. Source data are provided as a Source data file.
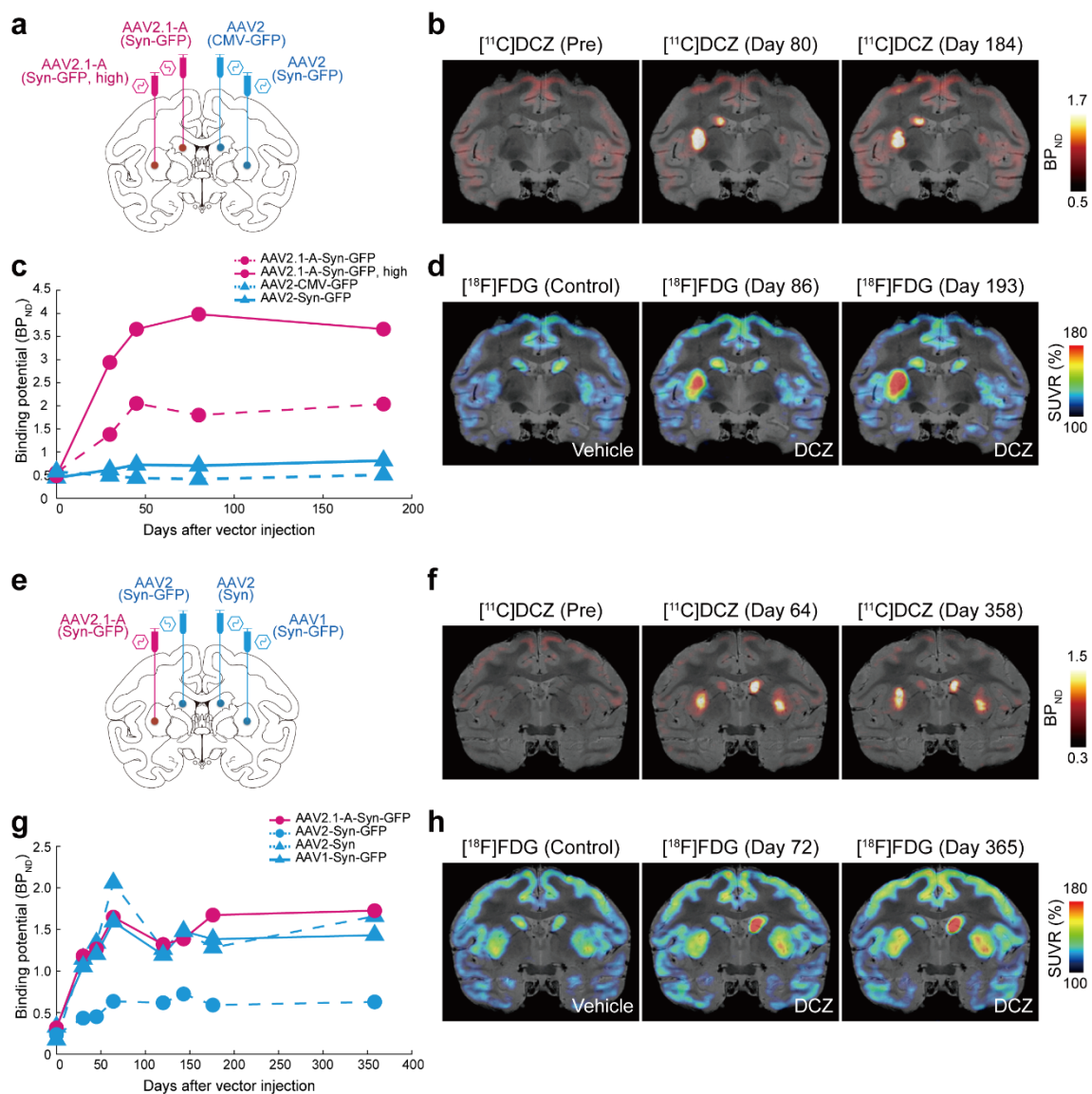
Fig. 2-5. Chemogenetic manipulation of striatal neuron activity.

(**a**) Schematic diagrams showing the sites of vector injections in the striatum in Monkey E. Four distinct vectors were injected into the striatum: AAV2.1-A-Syn-GFP into the caudate nucleus and the same vector at a higher titer (Syn-GFP, high) into the putamen on one side, and AAV2-CMV-GFP into the caudate nucleus and AAV2-Syn-GFP into the putamen on the other side. (**b**) Representative PET images overlaid on MR images showing [^{11}C]DCZ-specific binding taken before (Pre) or at 80 and 184 days (Day 80,

Day 184) after the vector injections. Each value of binding potential is expressed as the regional binding potential relative to a non-displaceable radioligand in tissue (BP_{ND}). (**c**) Time-dependent changes of [^{11}C]DCZ-specific binding at the sites of vector injections. Values before the injections, corresponding to (Pre) in (**b**), are plotted at Day 0. (**d**) Representative PET&MR-fused images showing normalized [^{18}F]FDG uptake following vehicle administration (Control) or DCZ administration at 86 and 193 days (Day 86, Day 193) after the vector injections. Each value of FDG uptake is expressed as the standardized uptake value ratio (SUVR) to the mean value of the whole brain, averaged between 60 and 90 min after the radioligand injection. (**e**) Sites of vector injections in the striatum in Monkey F. Four distinct vectors were injected into the striatum as follows: AAV2-Syn-GFP into the caudate nucleus and AAV2.1-A-Syn-GFP into the putamen on one side, and AAV2 vector with Syn promoter but without GFP tag (AAV2-Syn) into the caudate nucleus and AAV1-Syn-GFP into the putamen on the other side. (**f**) Representative PET images overlaid on MR images showing [^{11}C]DCZ-specific binding (expressed as BP_{ND}) taken before (Pre) or at 64 and 358 days (Day 64, Day 358) after the vector injections. (**g**) Time-dependent changes of [^{11}C]DCZ-specific binding at the sites of vector injections. Values before the injections, corresponding to (Pre) in (**f**), are plotted at Day 0. (**h**) Representative PET&MR-fused images showing normalized [^{18}F]FDG uptake (expressed as SUVR) following vehicle administration (Control) or DCZ administration at 72 and 365 days (Day 72, Day 365) after the vector injections. Source data are provided as a Source data file.
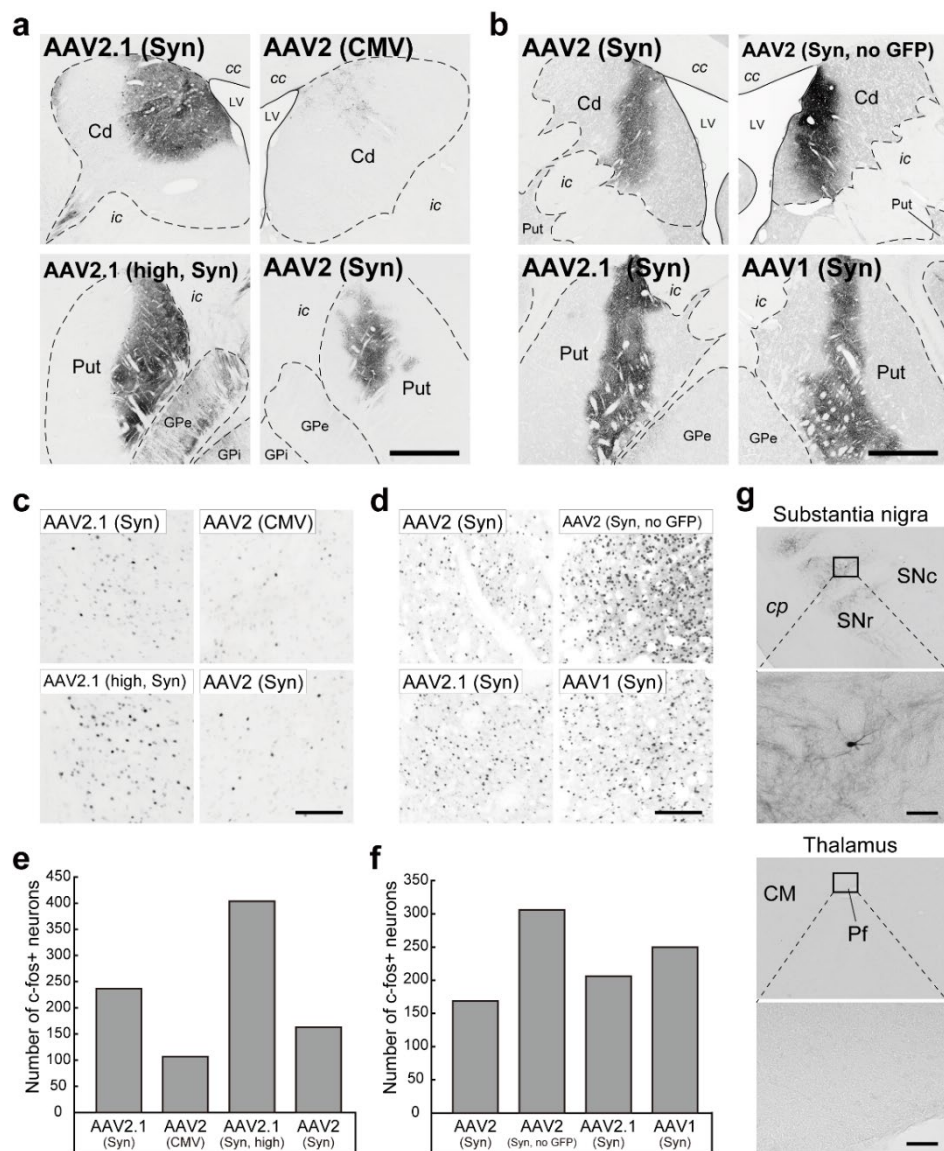
Fig. 2-6. Histological analyses of striatal sections subjected to chemogenetic manipulation.

(**a,b**) Sites of vector injections immunostained with anti-GFP (a) or anti-M3 (b) antibody in Monkeys E and F, respectively. Coronal sections. Scale bar, 1 mm. cc, corpus callosum; Cd, caudate nucleus; GPe, external segment of the globus pallidus; GPi, internal segment of the globus pallidus; ic, internal capsule; LV, lateral ventricle; Put, putamen. (**c,d**) Immunostaining for c-fos at individual vector injection sites corresponding to (**a,b**). Scale

bar, 100 μm. (**e,f**) Number of c-fos-positive neurons within a 1-mm-diameter circular observation window at individual vector injection sites corresponding to (**a,b**). Expressed as the mean value of cell counts obtained from three equidistant sections. The cell counts were done over the whole transgene-expressing region within the Cd or Put in each section. The averaged number of c-fos positive neurons at the densest area is chosen as a representative value. See the Methods for the details of cell-count analysis. (**g**) GFP immunostaining showing anterograde labeling in the substantia nigra pars reticulata (SNr, upper) and thalamus (lower) on the side ipsilateral to the AAV2.1-A vector injection. Anterograde axonal labeling is also seen in the GPe and GPi in the lower-left panel of (**a**). Only a single neuron is retrogradely labeled in the substantia nigra pars compacta (SNc). Data were obtained in Monkey E. CM, centromedian thalamic nucleus; cp, cerebral peduncle; Pf, parafascicular thalamic nucleus. Scale bars, 100 μm. Source data are provided as a Source data file.
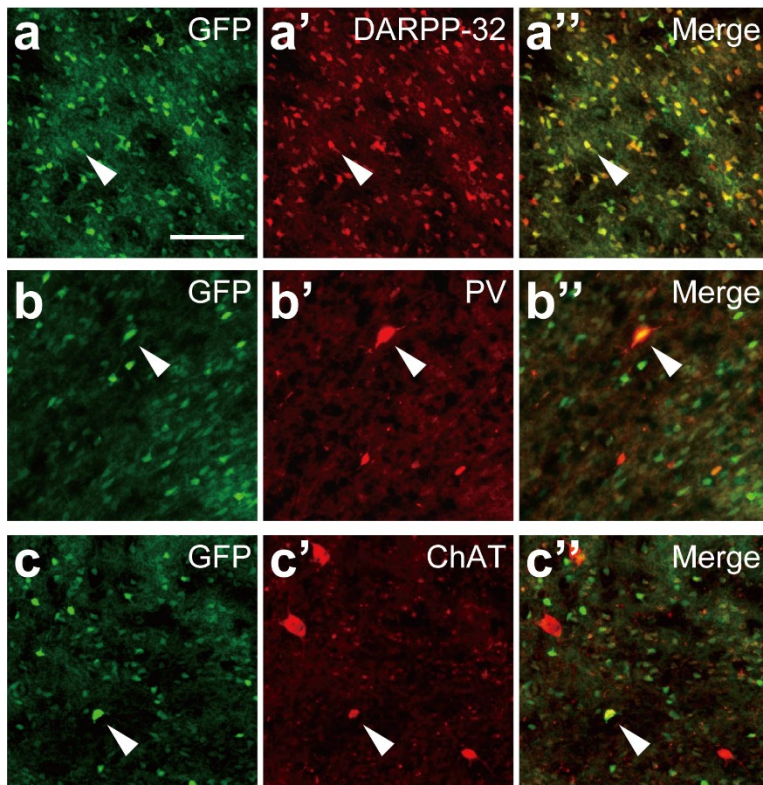
Fig. 2-7. Cell types of striatal neurons transduced with AAV2.1-A vector.

Double fluorescence histochemistry for GFP native-fluorescence (green; a-c) and immunofluorescence for DARPP-32, PV, or ChAT (red; a'-c') at the site of AAV2.1-A vector injection in the striatum. Data were obtained in Monkey E. Shown in yellow (Merge; a"-c") are double-labeled neurons which are pointed to with arrowheads. Scale bar, 100 μm.
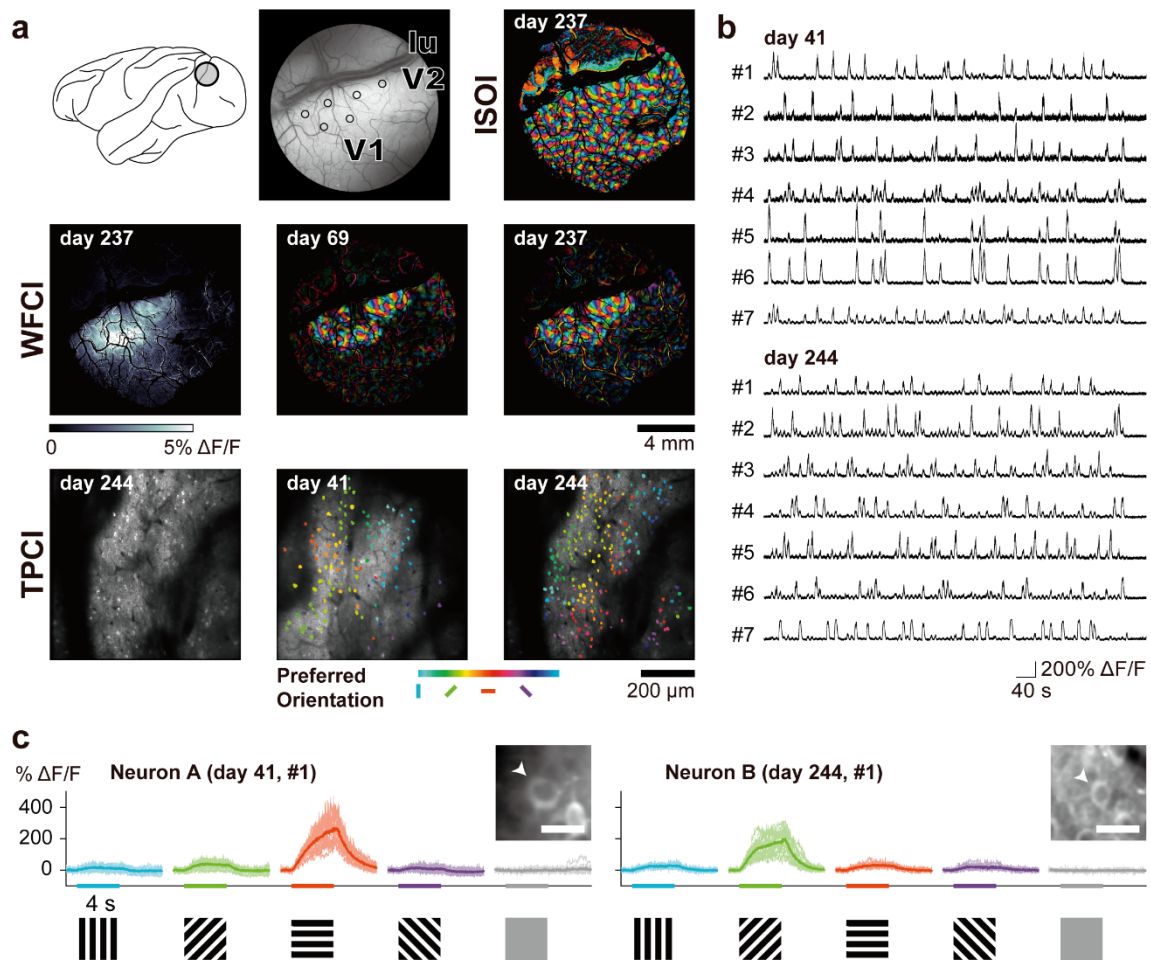
Fig. 2-8. *In vivo* calcium imaging of visual cortical neuron activity.

(**a**) Upper row: Left, a recording chamber placed over the V1 and V2 in Monkey H; Central, six loci of AAV2.1-A vector (AAV2.1-A-CaMKIIα-GCaMP6s) injections (denoted by open circles). lu, lunate sulcus; Right, intrinsic signal optical imaging (ISOI) for visualizing an orientation map of the visual cortex at 237 days post-injection. Middle row: One-photon wide-field calcium imaging (WFCI). Left, vector injection sites at 237 days post-injection visualized by selecting the maximum fluorescence changes ($\Delta F/F$) for each pixel across all stimulus conditions; Central & Right, orientation maps visualized at 69- and 237-days post-injection. The color code indicates the preferred orientation determined for each pixel. Note that these maps are basically consistent with the one

obtained from ISOI (see the upper right) and, also, at the two timepoints apart about six months. Lower row: Two-photon calcium imaging (TPCI). Left, structural image of the recording sites at 244 days post-injection obtained by averaging the fluorescence across all frames for a recording session. Central & Right, orientation maps at the single-neuron resolution at 41- and 244-days post-injection. The color code represents the preferred orientation determined for each neuron. (**b**) Time-dependent changes ($\Delta F/F$) in fluorescent signals obtained from 14 exemplified neurons in the V1 recorded at 41 and 244 days after the vector injection. These calcium transients were recorded in response to visual stimuli. (**c**) Responses of fluorescent signals of two V1 neurons (Neurons A and B) to drifting gratings of different orientations. The responses to the same orientation with opposite moving directions are superimposed. (Insets) Arrowheads point to the imaged neurons with typical nucleus-empty appearance of GCaMP labeling. Data were obtained in Monkey H. Scale bars, 20 µm.
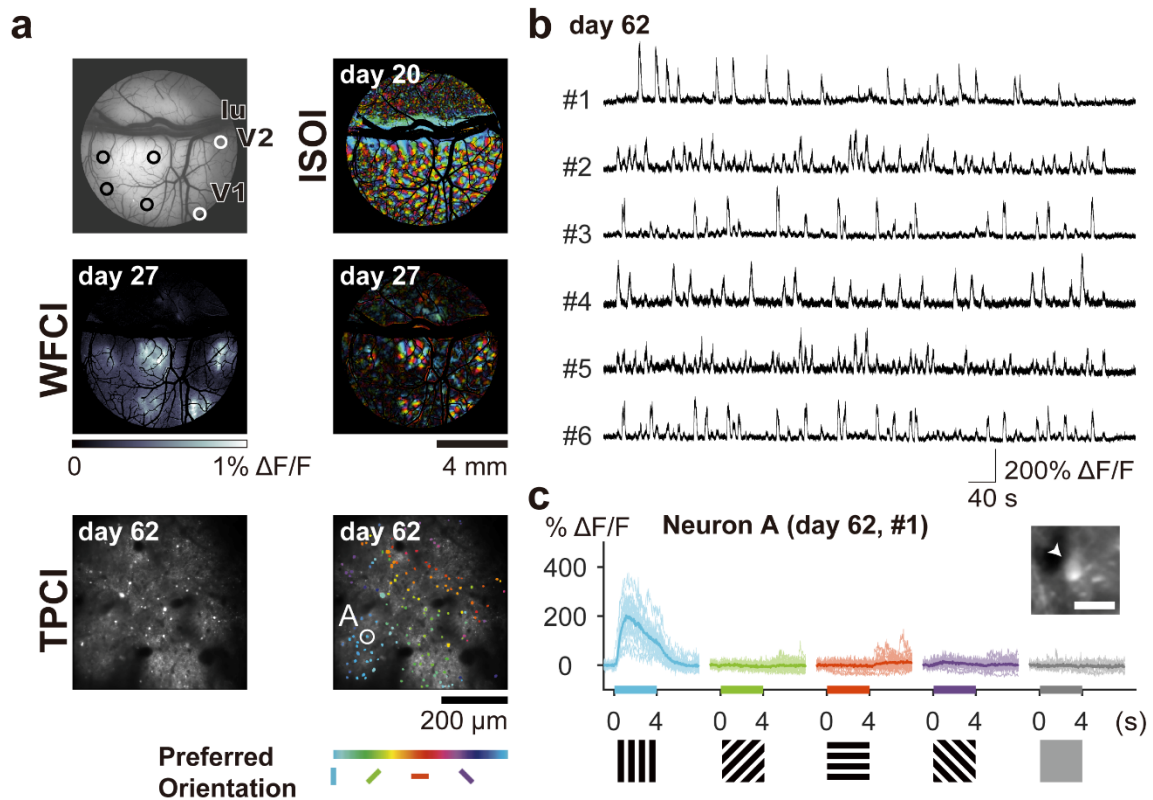
Fig. 2-9. *In vivo* calcium imaging of visual cortical neuron activity for determining optimal conditions.

(**a**) Upper row: Left, six loci of GCaMP6s-expressing AAV2.1-A vector injections (denoted by open circles; AAV2.1-A-CaMKIIα-GCaMP6s in black, AAV2.1-A-Syn-GCaMP6s in white) in Monkey G. lu, lunate sulcus; Right, intrinsic signal optical imaging (ISOI) for visualizing an orientation map of the visual cortex at 20 days post-injection. Middle row: One-photon wide-field calcium imaging (WFCI). Left, vector injection sites at 27 days post-injection visualized by selecting the maximum fluorescence changes ($\Delta F/F$) for each pixel across all stimulus conditions; Right, orientation map visualized at 27 days post-injection. The color code indicates the preferred orientation determined for each pixel. Note that this map is basically consistent with the one obtained from ISOI (see the upper right). Lower row: Two-photon calcium imaging (TPCI). Left, structural image

of the recording sites at 62 days post-injection obtained by averaging the fluorescence across all frames for a recording session. Right, orientation map at the single-neuron resolution at 62 days post-injection. The color code represents the preferred orientation determined for each neuron. (**b**) Time-dependent changes ($\Delta F/F$) in fluorescent signals obtained from six exemplified neurons in the V1 recorded at 62 days after the vector injection. These calcium transients were recorded in response to visual stimuli. (**c**) Responses of fluorescent signals of a V1 neuron (Neuron A) to drifting gratings of different orientations. The responses to the same orientation with opposite moving directions are superimposed. (Inset) Arrowhead points to the imaged neuron. Data were obtained in Monkey G. Scale bar, 20 µm.
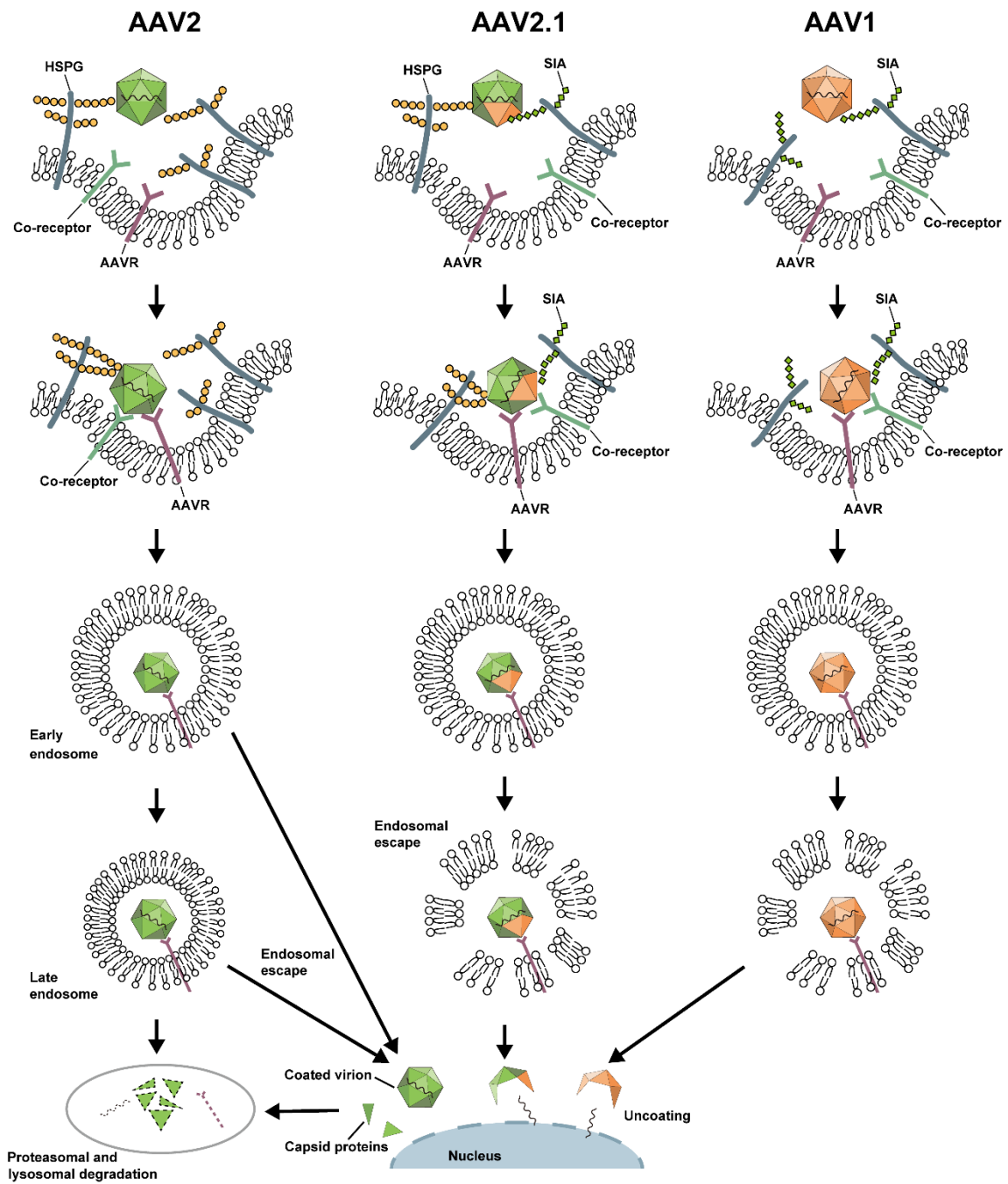
Fig.3-1 Hypothesis of trafficking process of AAV2.1 vector into nucleus

The schematics of trafficking process of the AAV2.1 vector, the AAV2 vector and the

AAV1 vector into the nucleus. Upper row, binding of AAV to heparan sulfate

proteoglycan (HSPG) or sialid acid (SIA) for the first entry into the host cell. The AAV2

vector is bound to heparan sulfate proteoglycan (HSPG) and the AAV1 vector is bound to SIA. The AAV2.1 vector can be bound by both HSPG and SIA. The AAV vectors enter the cell through endocytosis with the support of bindings by co-receptor and AAV receptor (AAVR). After endocytosis process, endosome internalizing AAV particle is trafficked to nucleus. Before degradation of endosome by lysosome, AAV particle escapes from endosome. In previous research, it is reported that AAV2 capsid has lower efficiency to escape from endosome. In addition, uncoating efficiency of AAV2 is lower than that of AAV1. This indicated that the AAV2.1 vector also has high efficiency of endosomal escape and uncoating, and these characteristics of AAV1 capsid allows the high efficiency of gene transduction. HSPG, heparan sulfate proteoglycan; SIA, sialic acid; AAVR, AAV receptor.